C.P. No. 1279

C.P. No. 1279

PROCUREMENT EXECUTIVE, MINISTRY OF DEFENCE

AERONAUTICAL RESEARCH COUNCIL

CURRENT PAPERS

Comparison between Dynamic Stability Boundaries for NPL 9615 and NACA 0012 Aerofoils Pitching about the Quarter - Chord

by

A. W. Moore, N. C. Lambourne and L. Woodgate

Aerodynamics Dept., R.A.E., Teddington

LONDON: HER MAJESTY'S STATIONERY OFFICE

1974

PRICE 85p NET

UDC 533.69 : 533.6.013.412

CP No.1279 *
August 1971

COMPARISON BETWEEN DYNAMIC STABILITY BOUNDARIES FOR NPL 9615 AND NACA 0012 AEROFOILS PITCHING ABOUT THE QUARTER-CHORD

by

A. W. Moore
N. C. Lambourne
L. Woodgate

SUMMARY

The results are presented of stall flutter tests on two aerofoils one with NACA 0012 section and the other with NPL 9615 section. A free-oscillation technique is used, each model having a single degree of freedom, namely pure pitching about a quarter-chord axis. Conditions giving zero aerodynamic damping are found for a range of frequency, Mach number, mean incidence and amplitude of oscillation appropriate to a helicopter blade. The results with a smooth leading edge are seen to compare favourably with other tests in which forces were determined by integration of chordwise pressure distributions measured near the centre line of a similar aerofoil.

The main conclusion from these tests, reached after a consideration of the relative positions of the boundaries for negative aerodynamic damping and for maximum lift, is that the improvements that the NPL 9615 section offers in maximum lift can be used with no greater likelihood of stall flutter occurring with this section than with the NACA 0012 section. A further important conclusion relates to the condition of the leading edge. When a roughness strip of carborundum particles is added at the leading edge of each aerofoil, instability is encountered at a lower mean incidence than with a smooth surface.

---

* Replaces RAE Technical Report 71163 - ARC 33252

CONTENTS

1 INTRODUCTION

In recent years there has been a growing interest in the aerodynamics of helicopter blades. This has included the derivation of new profiles aimed at improving performance and eliminating some of the vibrations that stem from disorderly flows. In the United Kingdom, for example, the approach has been to evolve suitable modifications to the much used NACA 0012 section. The environment encountered by a rotor blade in forward flight is strongly time dependent and threedimensional; nevertheless, the local loads and their chordwise distributions are closely similar to those on aerofoils in steady flow provided that the flow is attached and that strong vortex interactions are absent. It is hardly surprising therefore that certain beneficial trends shown by the steady-flow tunnel tests also occur in flight. However, in the presence of separated flow, a knowledge of the dynamic behaviour becomes essential. For instance, it is well known that with an oscillating aerofoil the static stall angle can be exceeded momentarily with an associated increase in lift. This lift 'benefit' might vary with different sections, and it is also possible that changes in the dynamic stalling behaviour of different sections could adversely affect aerodynamic damping characteristics and thus the likelihood of encountering stall flutter with its associated divergent vibratory loads.

The possibility of stall flutter exists for those combinations of Mach number and incidence for which the aerodynamic pitching-damping is negative. For the forward flight condition, such combinations may be experienced by a portion of the blade over sector of the azimuth without incurring disastrous results from flutter; nevertheless the cyclic appearance of negative aerodynamic damping should be avoided since it may lead to undesirable increases in cyclic loads and vibrations. Fundamental aspects of the dynamic stalling behaviour of aerofoils under conditions appropriate to those met by a section of a rotor blade in forward flight are to be examined in an extensive programme due to begin shortly. The work described in the present Report is an investigation addressed solely to the stall flutter properties of the NPL 9615 aerofoil section which is a drooped nose derivation of the NACA 0012 section and gives significant increases in maximum lift in comparison with the symmetrical aerofoil[1]. The present tests were planned to check that the dynamic stability of the NPL 9615 under maximum lift conditions is no worse than that of the NACA 0012. To this end, stability boundaries in the Mach number, mean incidence - i.e. (M, α) - plane have been determined for a range of frequencies and

amplitudes of oscillation. The effects of a roughness band of carborundum particles around the leading edge of each of the aerofoils have also been examined.

2 METHOD

For simplicity, a free-oscillation technique was chosen; this entailed only slight modifications to an existing derivative rig capable of being used in the 36in × 14in tunnel (91cm × 36cm) at Teddington which operates with atmospheric stagnation pressure. The method consisted of releasing the model from an initial deflection about a pitching axis and recording the subsequent motion; the overall pitching-damping was derived from the records. Pressure plotting along a chordwise station at mid-span during forced oscillations would have been more satisfactory from the point of view of minimizing side-wall effects on the measurements, but the simpler method using existing apparatus seemed justified on the grounds of expediency since the prime purpose was to compare the characteristics of two aerofoils. As a check on the validity of the method it was possible to compare the results obtained for the NACA 0012 section with those obtained at Boeing Vertol[2-4] using a more elaborate method.

2.1 Oscillating rig

The basic rig is denoted as Rig 4 in Ref.5, and was designed to produce resonant oscillations of constant amplitude with electrical feedback and with frequency determined by the stiffness of a torsion bar. For the present purpose, the driving coils were locked so that the torsion bar was effectively clamped to earth at one end. The other end of the torsion bar was rigidly attached to a cylinder mounted on cross springs as shown schematically in Fig.1. The tongue of the model was bolted onto a flange fitted to the end of the cylinder remote from the torsion bar. On the other side of the tunnel, the model was fixed to a carefully aligned cross-spring bearing. Metal 'boxes' attached to the tunnel walls sealed the apparatus from the atmosphere, and cover plates in the tunnel walls minimized transverse flow between the boxes and the tunnel.

Two safety devices were built into the rig on the torsion-bar side to limit the amplitude of any growing oscillation which might be encountered. Firstly, adjustable contacts on the moving cylinder operated a micro-switch at a preset amplitude to bring into action a quick-acting mechanical brake which

clamped on to the cylinder near to the point of attachment of the torsion bar. Secondly, should the brake fail to damp out the growing oscillation, then a projection on the moving cylinder came into contact with adjustable stops.

2.2 Initial deflection and trigger system

Provision was made for deflecting the model a preset amount about the pitching axis and then releasing it. In order to avoid excessive forces on the cross-spring bearings, the initial deflection was produced by the application of a couple from deflecting and trigger mechanisms. Each was a scaled-up version of an earlier design (see Ref.6) and consisted essentially of a cranked catch which was moved vertically by a hydraulic ram to engage on a shoulder and thereby apply a couple to the cylinder. The two shoulders which are not shown in Fig.1 were located near to the point of attachment of the cylinder to the torsion bar. On reaching a stop the catch was disengaged rapidly with the aid of a spring to ensure a quick release of the model; on releasing the hydraulic pressure another spring reversed the motion of the ram to reset the catch for subsequent displacement. The magnitude of the initial deflection could be changed by adjusting the position of each stop. It should be noted that the system for setting the mean incidence of the model was completely independent of the deflection and trigger system which determined only the initial amplitude of oscillation.

2.3 Models

Each model had a chord of 25.4 cm (10 in) and a span of 35.6 cm (14 in), the section shapes being NPL 9615 and NACA 0012 respectively. When mounted in the oscillating rig each model had a single degree of freedom, namely, a pure pitching motion about a quarter-chord axis. The models were mass-balanced about this axis to keep the inertial loads on the cross-springs to a minimum and were designed to be as rigid as possible. Alteration of mean incidence was achieved by rotation of the flanges to which the tongues of the model were attached. As indicated in Fig.2, each model was constructed from four components - a solid steel forward section with integral supporting tongues, Dural top and bottom portions forming a hollow centre-section, and a Dural trailing edge. The top and bottom halves of the centre-section were first electron-beam welded together and then fixed to the solid nose and tail by dowelled and Araldite-cemented joints prior to final machining.

Some dynamic tests at Boeing Vertol[2-4] in a pressurised tunnel reached full-scale Reynolds numbers with model chords of 16 cm; it is reported that when the Reynolds number was halved there were no consistent measurable differences in pitching damping. However, it is known from results with steady flow that simulation of full-scale chord Reynolds number is not, in itself, sufficient. The position of transition and the thickness of the boundary layer at the separation point are also relevant parameters. Since the surfaces of wind-tunnel models are usually far smoother than the surface of a full-scale rotor blade, tunnel tests at a full-scale Reynolds number might not give the required transition position. It has become the practice to artificially promote early transition on wind-tunnel models by adding a roughness band near to the leading edge, but the position and size of roughness must be carefully chosen so that the turbulent boundary layer so obtained is not too thick. In the present case, the transition point and boundary-layer thickness appropriate to a section of the full-scale blade are not known. It is not clear whether or not transition should be artificially fixed to obtain representative results. Measurements have therefore been made on both models with no transition band ('smooth surface') and with carborundum added around the leading edge ('roughness added'). To be consistent with steady-flow tests, the roughness band consisted of carborundum grains, size 0.05 mm to 0.06 mm, attached on the front 2% of the model, the band designated Type 4 in Ref.7.

2.4 Data acquisition

A variable air condenser, in which the moving vanes were displaced with the model, formed a pick-up which was used with Southern Instruments FM equipment to give a voltage proportional to angular displacement. This voltage was recorded on magnetic tape together with a voice channel identifier. The recorded oscillation was analysed by Bratt's electronic integration method, described in section 5.1.1 of Ref.8, to give a value of the local logarithmic decrement, or logarithmic increment, and hence a value of aerodynamic damping. The aerodynamic stiffness was determined by measuring directly the change in frequency of oscillation from still-air to wind-on conditions.

2.5 Procedure

The tests included variations in four parameters over the following ranges:-

Mach number	$0.3 \leqslant M \leqslant 0.6$
Frequency of oscillation	$36\ \text{Hz} \leqslant f \leqslant 67\ \text{Hz}$
Initial displacement	$0.5^{\circ} \leqslant \theta_0 \leqslant 3.5^{\circ}$
Mean incidence	$8^{\circ} \leqslant \alpha \leqslant 16^{\circ}$

These have been set out in the order of 'ease of variation', it being possible to cover the range of Mach number in a single run. For most of the runs the frequencies used were 43 Hz, 58 Hz, and 67 Hz which, after application of the appropriate scale factor, correspond approximately to frequencies of 5.5/rev, 7/rev and 8/rev for a full-scale blade. Some additional tests were done with frequency 36 Hz, which corresponds to about 4.5/rev. The torsion bar with stiffness 2.278×10^4 N m/rad gave a natural frequency in still air of 67 Hz; the values 58 Hz and 43 Hz were obtained by adding inertia to the system, and 36 Hz was obtained with a different torsion bar with stiffness 6.655×10^3 N m/rad. In a typical run the model was first set at a desired mean incidence, and the stops of the trigger system were adjusted such that the model would be released after being displaced to an angle about 3.5° less than its mean position. The trigger system was then operated with wind-off, and the resultant decaying oscillation of the model was recorded in order to obtain a value for apparatus damping. With wind-on, the chosen speed was obtained with the model clamped at its mean incidence and the clamp was then released to see whether a growing oscillation would occur. If the system were stable, the model was then displaced, released, and the ensuing motion recorded*.

To change the initial displacement, the sealing box was opened so that the displacements at which the triggers released could be adjusted and synchronised. This was sometimes time-consuming and to keep such changes to a minimum, the ranges of Mach Number and frequency for a fixed mean incidence were covered first with triggers set to release the model from displacement of about 3.5°. Certain conditions were met for which the motion was unstable when released from 3.5° displacement but was stable with zero displacement. These tests were repeated with a reduced displacement of about 2.5°, and for

*With a given setting of the tunnel control, the Mach number was to some extent dependent on the incidence, so that had the model been held displaced whilst getting on speed the wrong mean Mach number would have been obtained, e.g. for a damped motion the desired Mach number would be achieved only at the instant of release of the model.

conditions under which growing oscillations were again obtained, the initial amplitude was reduced to about 1^{o}. In a few cases a displacement of 0.5^{o} was tried.

The experimental programme outlined above was repeated with several values of mean incidence namely 9^{o}, 10^{o}, 12^{o}, 14^{o} for the NACA 0012 section and 10^{o}, 11^{o}, 12^{o}, 14^{o} for the NPL 9615 section with some additional tests at 8^{o} for the NACA 0012 section and 16^{o} for the NPL 9615 section.

3 PRESENTATION OF RESULTS

Apart from the fact that the frequencies of oscillation of the model, after making due allowance for the scaling factor, correspond to the practical range of natural frequencies for the full-scale blade in torsion, no attempt was made to represent the mechanical properties of the rotor blade. For the model, the inertia and elastic stiffness forces were much larger in relation to the aerodynamic forces than they would be for a blade. Thus the observed kinematic behaviour of the model following release cannot be taken to be representative of that of a blade, and, for this reason, information on this aspect will not be presented or discussed in detail. Suffice it to say that, in addition to the oscillations either decaying to a condition in which the aerofoil was stationary or growing until restricted by the mechanical stops, there were other forms of free motion in which oscillations would decay or grow to a stable limit cycle; such behaviour as indicated in Figs.3a and 3b was due to non-linearities in the aerodynamics. However, because of the overwhelming influence of the mechanical forces, all the oscillatory motions were essentially sinusoidal and describable by the expression $e^{\mu t} \sin \omega t$ provided the value of μ is allowed to vary slowly with time.

In the analysis of the experimental results, values of μ were obtained from measurements of the local rate of decay or growth at chosen amplitudes of oscillation and, from these values, equivalent linear damping coefficients were obtained. Subtraction of the mechanical damping that had been obtained by the measurement of decay rates in still-air yielded values of the aerodynamic damping for different amplitudes of oscillation. The aerodynamic stiffness and damping coefficients were defined by

$$\bar{C}_{m} = 2\theta(m_{\theta} + i\nu m_{\dot{\theta}}) \qquad (1)$$

where $\bar{C}_m$ is the complex nondimensional pitching-moment coefficient, θ is the pitching amplitude, ν is the reduced frequency parameter, m_θ is the pitching moment in phase with the displacement and $\nu m_{\dot{\theta}}$ is the pitching moment in quadrature with the displacement. Although the measurements were obtained from transients, it is unlikely that the values of the aerodynamic damping so determined differ significantly from the damping appropriate to maintained sinusoidal oscillations. In the present tests, the local damping coefficient, $m_{\dot{\theta}}$, was calculated from the local rate of growth or decay of the recorded transients at four values of the pitching amplitude, namely 3°, 2°, 1° and $\frac{1}{2}^\circ$. These were plotted against M for various mean incidences as illustrated in Fig.4 with cross plots of $m_{\dot{\theta}}$ against α for various Mach numbers as in Fig.5. Values of M and α for zero damping are picked off these curves and hence stability boundaries for each of the four pitching amplitudes are obtained in an (M, α) plane as loci of conditions for zero damping.

Values of the stiffness derivative are given in Table 1, but their accuracy is poor. It was found during the course of the tests that the repeatability of the wind-on frequency of oscillation for given conditions was at best ±0.1%. Since the larger changes in frequency from still-air to wind-on conditions were about 1% of wind-on frequency, the stiffness derivative can, at best, be accurate to only ±10%; so the results in Table 1 should be treated with caution. For this reason no discussion of aerodynamic stiffness is given in later sections. It was not possible to detect any dependence on amplitude of oscillation, but there appears to be a general trend for rearward movement of the centre of pressure with increase of Mach number or mean incidence as would be expected from steady flow results.

Values of the damping derivative are given in Tables 2 to 5.

4 DISCUSSION

The scope of the experiments has been outlined in section 2.5 and covers a range of Mach number, mean incidence, amplitude of oscillation and frequency of oscillation. Furthermore, measurements were made both with and without a roughness band on each model. We first consider the general behaviour of the damping coefficient of the aerofoils, after which the effect of individual parameters on the loci of zero damping in the (M, α) plane is discussed.

4.1 General form of the variation of damping coefficients

The damping coefficient $m_{\dot{\theta}}$ is found to change very abruptly with incidence and Mach number over certain ranges. The influences of amplitude and

of frequency of oscillation, and the effect of roughness applied to the leading edge, are each less dramatic and are conveniently considered as modifications to the basic variations with Mach number and incidence. Figs.4 and 5 show examples of $m_{\dot{\theta}}$ plotted against M and α to illustrate the variety, but not the entirety, of forms encountered in the investigation. We shall later find it convenient to discuss the results in terms of the particular boundary in the (M, α) plane corresponding to $m_{\dot{\theta}} = 0$ which represents the dynamic stability boundary for the pitching of the aerofoil. Before doing so, however, it may be helpful to illustrate the general form of the variation of $m_{\dot{\theta}}$ over the (M, α) plane by a brief description of the general topography of such a threedimensional representation as deduced from a survey of the present experimental results and as illustrated schematically by the contours shown in Fig.6.

Outwards from the origin (M = 0, α = 0) it is reasonable to assume that $(-m_{\dot{\theta}})$ remains fairly constant although showing some rise with increasing Mach number. This plateau is intersected by a valley corresponding to a steep drop in damping to a negative value. It is plausible to associate the slight rise above the plateau value that occurs before the near side of the valley is reached with the development of compressibility effects, and the abrupt fall in damping with the appearance of separation. Attention in the present experiment has been concentrated on the nearer edge of this valley since this is of greater practical importance, but there is enough information to indicate that the damping can rise to large positive values on the farther side.

With regard to the primary purpose of the investigation, comparison between the characteristics of the NPL 9615 and the NACA 0012 sections shows a change in the position of the negative damping valley, but no significant difference in the steepness of its sides. The change in its position will be discussed more fully in section 5.

For both aerofoils, changes of amplitude and frequency of oscillation appear to have no significant effect on the plateau value of $(-m_{\dot{\theta}})$. An increase in amplitude results in a shift in the position of the valley to lower values of M and α, and a general rounding off of the topography so that the valley becomes wider but less deep. An increase of frequency tends to decrease the steepness of the valley and to shift its position to somewhat higher values of M and lower values of α.

With the roughness band added at the leading edge, the valley tends to move to lower values of M and α, this effect being more noticeable for smaller amplitude.

The remainder of the discussion refers almost exclusively to the position of the $m_{\dot{\theta}} = 0$ contour in the (M, α) plane since this serves as a convenient indicator of the region in which the damping is severely reduced from its normal value. Diagrams plotted in the (M, α) plane are frequently used to display steady motion boundaries such as C_{Lmax} for an aerofoil, and these diagrams are relevant to a consideration of the cyclic conditions met by sections of a rotor blade in the forward flight case. For the present investigation, plots of the $m_{\dot{\theta}} = 0$ contour in the (M, α) plane provide a rapid means of assessing the influence of various factors on the stability of a section with regard to stall flutter.

The results suggest that the general form of this contour, which encloses a region of negative damping as shown in Fig.7 consists of a lower portion A, a nose B and an upper portion C. This is in general agreement with the form of the boundaries shown by Liiva and Davenport[3]. In broad terms, the lower portion A of the boundary corresponds to the incidence below which only positive damping occurs, the upper portion C to incidences above which the damping is again positive. The nose B defines a Mach number above which the damping will be positive for all incidences. The position of the negative damping region in the (M, α) plane depends on frequency and amplitude of oscillation and on whether or not roughness is added at the leading-edge of the aerofoil. The influence of these factors will be discussed in the following sections. For some conditions neither the nose nor the upper boundary come within the ranges of Mach number and incidence covered by the experiments.

Since we shall use the C_{Lmax} curve as a landmark in the (M, α) plane, it is necessary to appreciate the arbitrary nature of the relationship between this line and the $m_{\dot{\theta}} = 0$ contour. For increasing incidence at constant Mach number we would expect the value of $m_{\dot{\theta}}$ to begin to change close to the point where the C_L vs α curve departs from linearity and where radical changes first make their appearance in the pitching moment, since each of these changes is due to the onset of separation. However, the decrease of $-m_{\dot{\theta}}$ to zero would require a further increment of incidence; so also would the attainment of C_{Lmax}. But there is of course no *a priori* reason for regarding these increments as identical and thus no reason to associate precisely the condition $m_{\dot{\theta}} = 0$ with the incidence for C_{Lmax}.

4.2 Effect of amplitude

Figs.8 to 11 show stability boundaries for the NACA 0012 and NPL 9615 sections with and without a roughness band for various amplitudes. For a given frequency it is clear that the Mach number for zero damping varies with amplitude of oscillation, and, particularly for the lower portions of the stability loops away from the minima, there is a nearly linear dependence of the Mach number on amplitude of oscillation. The sense is such that when amplitude is increased with fixed frequency and mean incidence, instability occurs at a lower Mach number: alternatively, with fixed frequency and Mach number, increased amplitude leads to instability at a lower mean incidence. For low speeds, $M < 0.5$ say, the effect of amplitude of oscillation on the occurrence of negative damping implies that there is a possibility of unstable limit cycles in practice; in other words 'hard oscillator' characteristics can exist whereby stall flutter can be precipitated by an impulse but will not occur if there is no disturbance.

Fig.8 (mid) includes a stability boundary for the NACA 0012 section given by Liiva and Davenport[3]. This curve was derived from the results of Boeing Vertol tests in which a twodimensional aerofoil was driven in a pitching mode of oscillation*. Instantaneous pressures were measured at thirteen chordwise positions distributed along two lines near to the centre line of the model. The data are presented in Ref.2. The majority of tests were done with a 5^{o} oscillation amplitude for a model with 16 cm chord. A few additional measurements were made with amplitudes 2.5^{o} and 7.5^{o}, and for one Mach number the incidences for zero damping can be obtained for all three amplitudes. The variation in α for zero damping confirms the near linear dependence on amplitude found in the present tests. It happens that some of the measurements described in Ref.2 were done with a frequency parameter, $\omega c/V$, which varied from 0.97 to 0.49 as the Mach number varied from 0.3 to 0.6. This is similar to the range of frequency parameter achieved in the present tests with 58 Hz, for which $\omega c/V$ varies from 0.92 to 0.47.

Extrapolating the present results to a 5^{o} oscillation amplitude on a linear basis gives a boundary in reasonable agreement with the Boeing Vertol

---

*The aerofoil used in the Boeing Vertol tests was actually a modified form of the NACA 0012; according to Ref.4 the modification consisted of a symmetrical leading-edge fairing (corresponding to a typical anti-icing boot) and a flat sheet-metal trailing-edge extension.

results. This implies that the present measurements of overall damping on the complete aerofoil, as distinct from pressure measurements at the centre section, give stability boundaries which are not severely influenced by end-effects. The possibility of threedimensional effects as described in Ref.9 had previously raised some doubts regarding the validity of overall force measurements, but the agreement with the Boeing Vertol results is taken as justifying the method, at least for a comparison of aerofoil sections.

4.3 Effect of frequency

The influence of frequency is conveniently shown by the stability boundaries plotted in Figs.12 to 15.

Frequency has a significant effect on the position of the nose of the boundary; increase of frequency moves it to higher Mach number and lower mean incidence. At the same time the loop is broadened by a displacement of the upper boundary. The effect on the lower side of the boundary is smaller, especially when the leading edge is smooth; the changes that do occur at low Mach numbers are such that an increase in frequency delays the onset of negative damping to a higher incidence. These observed changes in the boundary lead to an important consideration: whereas at low Mach numbers it may generally be beneficial to the prevention of stalling flutter to raise the torsional frequency of a blade, such a change may be deleterious at higher Mach numbers.

It might be noted that, from a practical point of view, the operating line for a section of a rotor blade is not likely to approach the upper portion of the boundary except near the nose.

4.4 Effect of leading-edge roughness

The effect of a roughness band on the leading edge of the NACA 0012 and NPL 9615 sections is shown in Figs.16 to 19. In general, for a given frequency and amplitude of oscillation roughness enlarges the region of negative damping. The lower portion of the boundary is lowered, the nose is moved to the right and the upper portion is raised; physically, this means that for a given mean incidence instability is encountered at a lower Mach number with the addition of roughness and persists to a high Mach number. An important practical implication is that if a rotor blade is designed to operate under conditions close to the stability boundary, then any deterioration in the smoothness of the blade surface might lead to the occurrence of stall flutter under conditions where it did not previously occur.

With reference to Figs.12 to 15, it appears that there is a much larger effect of frequency on the lower part of the boundary when the leading edge is roughened, and there is a tendency for roughness to have a greater effect at the lower frequencies.

4.5 Wind-tunnel interference

From past experience of the measurement of oscillatory pitching-moment derivatives in ventilated tunnels[10], it is known that results from tests on threedimensional models can be subject to large wall-interference effects. This is probably also true of twodimensional tests although no substantive measurements are known to the authors. However, the 36 in × 14 in (91 cm × 36 cm) with slotted liners was found to give negligible interference at subsonic speeds in tests with threedimensional models having quite large aspect ratios, so interference effects in the present tests are probably small. But even if wall interference is present it is likely that the results for the two aerofoils would be equally affected so that comparisons of the aerofoil characteristics would be valid. Again because only a comparison between sections was sought, no attempt was made to investigate, or alleviate, possible effects due to the tunnel side-wall boundary layers in which the ends of the models were immersed. As mentioned in section 4.2, the favourable comparison between results from the present tests with NACA 0012 and measurements of pressure distributions at the centre line of a similar model indicates that the influence of the side walls on modal damping characteristics was probably small.

5 RELATIVE PERFORMANCE OF THE TWO SECTIONS

The primary aim of the present tests was to obtain information on the damping in pitch properties of the NPL 9615 section and therefore an indication of the likelihood of the occurrence of stall flutter with blades having this section. Figs.20 to 23 show comparisons between the stability boundaries for the NPL 9615 and NACA 0012 sections for the largest amplitude of oscillation used in the tests and for zero amplitude of oscillation, the curves for the latter being obtained by extrapolation.

Also shown in these diagrams are C_{Lmax} loci for the two aerofoil sections. These loci have been obtained in the following manner. The steady measurements made by Gregory and Wilby[1] in the same wind-tunnel yield C_{Lmax} boundaries for both sections but with roughness applied to the leading edges

and with the top and bottom tunnel walls having a reduced open area ratio appropriate for steady tests. Subsequent tests by J. Osborne[11] on an aerofoil of NACA 0012 section have shown that for the wall condition used in the present tests the nominal incidence for C_{Lmax} would be raised by approximately 1 degree whilst without roughness the boundary would be raised by a further 0.1 to 0.2 degree. There is no reason to doubt that the effect of the change in wall condition would apply equally to the C_{Lmax} boundary for the NPL 9615 section. Thus for the purposes of the present comparison the loci obtained by Gregory and Wilby have been raised uniformly by 1.2 degrees in Figs.20 and 21, and by 1 degree in Figs. 22 and 23 in order to be consistent with the conditions under which the $m_\theta = 0$ boundary was obtained.

With a rotor, the likelihood of stall flutter occurring in the condition of forward flight is expected to depend on the relative disposition in the (M, α) plane of the region for negative damping and the operating loops for appropriate radial positions along the blade. In practice the C_{Lmax} line has been used as a criterion for limiting conditions so that, without the need to consider the whole family of loops for a range of operating conditions, a rapid assessment of the stall flutter characteristics of an aerofoil section can be made by considering the position of the C_{Lmax} line in relation to the negative damping region. When such a comparison is made as in each of Figs.20 to 23 we are led to the conclusion that the likelihood of stall flutter is no greater with the NPL 9615 than with the NACA 0012. Thus the performance gains stemming from the modified section are not likely to be jeopardized by a greater propensity for stall flutter.

6 CONCLUSIONS

(1) The main conclusion from the tests, reached after a consideration of the relative positions of the boundaries for negative aerodynamic damping and for maximum lift in the (M, α) plane, is that the improvements that the NPL 9615 section offers in maximum lift can be used with no greater likelihood of stall flutter occurring with this section than with the NACA 0012 section. This conclusion can be drawn from the results obtained with roughness added around the leading edge of each aerofoil as well as from the results obtained with smooth models.

(2) The onset of instability occurs at a lower angle of incidence when roughness is added near the leading edge of each aerofoil than when the surfaces are smooth. This implies that if a rotor blade is designed to

operate under conditions close to the stability boundary, then any deterioration in the condition of the blade surface might lead to stall flutter under conditions where it did not previously occur.

(3) An increase in the amplitude of oscillation leads to a decrease in the mean incidence at which instability is first encountered.

(4) For low speeds, an increase in the frequency of oscillation tends to increase the incidence for onset of instability. But for high Mach numbers, say $M > 0.5$, a decrease in frequency can completely eliminate the instability.

(5) For low speeds, $M < 0.5$ say, the effect of amplitude of oscillation on the occurrence of negative damping implies that there is a possibility of unstable limit cycles in practice; in other words 'hard oscillator' characteristics can exist whereby stall flutter can be precipitated by an impulse but will not occur if there is no disturbance.

(6) The general shape of the region of negative damping in the (M, α) plane agrees with that obtained from unsteady pressure measurements[2]. This agreement substantiates the free-oscillation technique involving total forces on the aerofoil model as a rapid assessment of pitch damping characteristics. But more detailed information about the dynamic stalling processes can only be obtained from measurement of instantaneous pressure distributions; such an investigation together with flow visualization is planned to start in the near future.

Acknowledgements

The tests were carried out at the National Physical Laboratory, Teddington during March and April 1970 before the aeronautical work at Teddington had been incorporated in the Aerodynamics Department, RAE.

The authors wish to acknowledge the valuable assistance of Mr. I. Lane and Mr. D. Nunn in carrying out the experimental programme. Mr. K.C. Wight advised on the use of the oscillating rig and Mr. J.B. Godwin designed the model displacement and rapid release system. The models were designed by Mr. P.T. Taylor and made by staff of the Model Workshop, NPL.

Table 1

VALUES OF STIFFNESS DERIVATIVE - m_θ

(a) 0012, smooth surface

M \ α	67 Hz				58 Hz			
	9	10	12	14	9	10	12	14
0.30	0	0	0	0	0	0	0	
0.35			0	0			0	0
0.40	0	0	0.66	-	0	0	0.69	0.01
0.45		0.05		-		0.18		
0.50	0.18	0.22	1.41	-	0	0.39	0.66	1.56
0.55	0.31	-	1.09	1.00	0.37	0.40	0.81	-
0.60	0.51	-	0.71	1.38	0.50	-	1.75	-

(b) 0012, roughness added

0.30	0	0	0	0	0	0	0	0
0.35		0	0			0	-	-0.14
0.40	0	0.13	-0.26	0.07	0	0	-0.40	0.18
0.45	0	0.22	-0.37		0	0.05		
0.50	0.09	0.18	0.98	1.11	0.27	0.39	0.73	1.82
0.55	0.39	0.44		0.87	0.51	0.55	0.72	0.99
0.60	0.87	0.77	1.08	0.86	0.53	0.90	0.84	1.08

(c) 9615, smooth surface

M \ α	67 Hz				58 Hz			
	10	11	12	14	10	11	12	14
0.30	0	0	0	0	0	0	0	0
0.35				0				0
0.40	0	0	0	0.98	0	0	0	0.22
0.45		0	0.26	0.43		0	0.14	0.61
0.50	0	0.18	0.44	0.72	0	0.27	0.39	0.66
0.55	0.15	0.38	0.65	0.84	0	0.43	0.60	1.42
0.60	0.60	0.64	0.81	1.83	0.52	0.76	1.09	1.43

(d) 9615, roughness added

0.30	0	0.11	0	0	-0.10		0	0
0.35				0.17			0	0
0.40	0	0.07	0.07	0.33	0	0	0.11	0.17
0.45			0		0.05	0.09	0.05	
0.50	0.05	0.04	0.36	0.96	0	0.29	0.43	0.55
0.55	0.15	0.27	0.56	1.46	0.43	0.44	0.62	0.61
0.60	0.28	0.52	0.59	0.68	0.41	0.53	0.65	0.78

Table 1 (concluded)

(a) 0012, smooth surface

M \ α	43 Hz				36 Hz			
	9	10	12	14	9	10	12	14
0.30	0	0.35	0	0				
0.35			0	0				
0.40	0			0.56				
0.45	0	0.42	0.24	1.20				
0.50	0	0.35	0.73					
0.55	0.32	0.71	0.80	-				
0.60	0.72	-	0.91	-				

(b) 0012, roughness added

0.30	0	0	-0.07	0.07				
0.35		0.05	0.11	0.50				
0.40	0.04	0	0.09	0.78				
0.45	0	0.30	0.58	0.96				
0.50	0.30	0.50	1.02	1.20				
0.55	0.45	0.51	1.40					
0.60	0.66	1.20	1.34	1.08				

(c) 9615, smooth surface

M \ α	43 Hz				36 Hz			
	10	11	12	14	10	11	12	14
0.30	0	0	0	0				
0.35			0	0.16				
0.40	0	0	0.08	0.43				
0.45		0	0.42	0.88				
0.50	0	0.17	0.52	0.76				
0.55		0.40	0.83	0.78				
0.60	0	0	0.91	0.81				

(d) 9615, roughness added

0.30	0	0	0		0	0	0.04	0
0.35			0			0	0.01	0.82
0.40	0	0	0.41	0.52	0	0.51	0.23	0.82
0.45	0	0.07	0.42	0.81	0.25	0.47	0.51	0.76
0.50	0	0.44	0.65	1.09	0.30	0.44	0.60	1.00
0.55	0.45	0.61	0.97		0.38	0.67	0.51	
0.60	1.00	1.03	1.42	1.00	0.79	0.85	0.75	1.05

Table 2

DAMPING DERIVATIVE - $m_{\dot{\theta}}$ FOR NACA 0012, SMOOTH SURFACE

(a) 3° oscillation amplitude

M \ α	67 Hz					58 Hz			
	8	9	10	12	14	9	10	12	14
0.30	0.457	0.431	0.377	0.428	0.015	0.506	0.402	0.514	0.044
0.35				0.300				-0.042	-1.265
0.40	0.688	0.666	0.252	-0.566	U	0.710	0.202	-0.731	
0.45			-0.213	-0.791	U			U	
0.50	0.416	0.026	-0.364	U	U	0.031	-0.383	U	-0.333
0.55		-0.039	U	U	-0.373	-0.156	U		0.026
0.60	-0.025	-0.073	U	-0.239	0.117	-0.076	U	0.239	0.121

(b) 2° oscillation amplitude

0.30	0.497	0.457	0.468	0.416	0.030	0.489	0.478	0.471	0.266
0.35				0.340				0.485	-0.356
0.40	0.781	0.623	0.577	-0.668		0.506	0.572	-0.946	U
0.45			0.349	-1.610	U		0.637	U	U
0.50	0.491	0.247	-0.404	U	U	0.272	-0.433	U	-0.668
0.55		-0.282	U	U	-0.629	-0.184	U	-0.595	0.007
0.60	0.041	-0.494	U	-0.493	0.068	-0.235	U	0.220	0.161

(c) 1° oscillation amplitude

0.30	0.552	0.532	0.418	0.486	0.094	0.458	0.478	0.508	0.345
0.35				0.441	-0.078			0.574	-0.699
0.40	0.847	0.583	0.615		U	0.544	0.646	-1.046	U
0.45			0.738	-1.527	U		0.794	U	U
0.50	0.499	0.974	0.254	U	U	0.727	0.395	U	-1.114
0.55		0.546		U	-1.100	0.797	U	-1.756	0.056
0.60	0.532	-1.213	U	-1.083	0.018	-1.156	U	0.485	0.207

(d) $\frac{1}{2}^{\circ}$ oscillation amplitude

0.30	0.464	0.584	0.483	0.458	0.094	0.465	0.440	0.527	0.389
0.35				0.481	-0.054			0.613	0.384
0.40	0.876	0.570	0.666	0.606	U	0.529	0.672	0.675	-2.890
0.45			0.836	-1.494	U		0.888	U	U
0.50	0.523	1.008	1.345	U	U	0.940	0.709	U	-1.574
0.55		0.577	U	U	-2.036	0.811	U	-2.728	0.083
0.60	0.768	-3.577	U	-1.931	-0.135		U	0.688	0.233

U indicates instability but no measurements made.

Table 2 (concluded)

(a) 3° oscillation amplitude

M \ α	43 Hz					
	9	10	11	12	13	14
0.30	0.255	0.655		0.500		
0.35				0		-0.998
0.40	0.483	0.168		-0.579		-0.621
0.45	0.528	-0.234		-0.218		0.230
0.50	0.066	0.145		0.369		0.665
0.55	0.032	0.424		1.144		1.303
0.60	0.277	0.823		1.527		1.217

(b) 2° oscillation amplitude

0.30	0.440	0.464		0.491		0.262
0.35			0.547	0.576		-1.460
0.40	0.564	0.613	-0.591	-1.579	-1.324	-1.126
0.45	0.647	0.279		-0.611	-0.213	0.075
0.50	0.319	-0.418	-0.061	0.285		0.705
0.55	0.129	0.056	0.703	1.216		1.340
0.60	0.298	0.878	1.111	1.595		1.252

(c) 1° oscillation amplitude

0.30	0.465	0.469		0.499		0.325
0.35			0.575	0.634		-2.992
0.40	0.522	0.680	0.704	0	-1.642	-3.238
0.45	0.654	0.874	-1.017	-1.689	-0.480	-0.350
0.50	0.814	0.552	-0.678	0.782	2.280	0.747
0.55	0.464	0.020	1.526	1.516	2.386	1.379
0.60	0.351	1.929	2.221	1.632	2.088	1.289

(d) $\frac{1}{2}^{\circ}$ oscillation amplitude

0.30	0.455	0.462		0.510		0.349
0.35			0.572	0.666	0.619	0.435
0.40	0.492	0.466	0.732	0.999	U	-6.477
0.45	0.610	0.907	0	-3.984	U	-0.620
0.50	0.756	0.884	-1.580	1.364	2.299	0.762
0.55	1.159	0.423	2.091	1.537	2.404	1.393
0.60	0.638	1.956	3.533	1.652	2.105	1.303

Table 3

DAMPING DERIVATIVE $-m_{\dot{\theta}}$ FOR NACA 0012 ROUGHNESS ADDED

(a) 3^{o} oscillation amplitude

M \ α	67 Hz				58 Hz				43 Hz			
	9	10	12	14	9	10	12	14	9	10	12	14
0.30	0.452	0.434	0.391	0.032	0.429	0.471	0.368	-0.088	0.409	0.500	0.130	-0.962
0.35		0.487	0.226			0.486	-0.124	-0.758		0.407		-1.532
0.40	0.516	0.150	-0.470	-0.895	0.518	0.028	-0.771	-1.131	0.390	-0.691	-1.206	-1.234
0.45	0.245	-0.425	-1.381		0.029	-0.643			-0.235	-0.624	-0.853	-0.408
0.50	-0.159	-0.739	-1.361	-1.251	-0.404	-0.876	-1.137	-1.023	-0.418	-0.508	0.161	0.319
0.55	-0.428	-0.923		-0.958	-0.501	-0.774	-0.822	-0.489	-0.235	-0.016	0.958	
0.60	-0.612	-0.731	-0.789	-0.436	-0.434	-0.475			0.205	0.687	1.461	2.184

(b) 2^{o} oscillation amplitude

0.30	0.427	0.446	0.433	-0.008	0.435	0.454	0.388	-0.161	0.424	0.512	0.450	-0.565
0.35		0.472	0.348			0.485	0.237	-0.717		0.495		-2.360
0.40	0.484	0.522	-0.359	-1.158	0.512	0.580	-0.719	-1.993	0.464	0.230	-1.975	-2.701
0.45	0.542	-0.292	-1.313		0.577	-0.510			0.610	-1.105	-1.398	
0.50	0.084	-0.902	-1.725	-1.931	-0.080	-1.166	-2.249	-1.702	-0.510	-1.142	-0.338	0.644
0.55	-0.569	-1.530		-1.808	-0.752	-1.397	-1.549		-0.486	-0.293	1.068	
0.60	-1.002	-1.842	-1.189		-0.682	-0.859		0.682	0.287	0.905	1.565	2.303

Table 3 (concluded)

(c) 1^{o} oscillation amplitude

M \ α	67 Hz				58 Hz				43 Hz			
	9	10	12	14	9	10	12	14	9	10	12	14
0.30	0.431	0.461	0.448	-0.407	0.450	0.461	0.435	-0.466	0.429	0.524	0.503	-0.597
0.35		0.499	0.427			0.481	0.332	-0.814		0.486	0.452	-1.692
0.40	0.483	0.550	0.050	-1.681	0.501	0.529		-2.143	0.487	0.646		-3.211
0.45	0.581	-1.036	-1.048		0.591	0.685			0.598	0.757	-5.147	2.286
0.50	0.639		-2.819	-1.896	0.465	-1.838	-4.191		0.694	-1.621	-1.376	2.167
0.55	-0.620	-2.497		-0.481	-0.726	-3.566	-3.215		-0.942	-0.835	2.567	
0.60	-1.816	-3.101	-4.954	0.669	-1.538	-1.131		1.324	0.676	2.189	1.908	2.346

(d) $\frac{1}{2}^{o}$ oscillation amplitude

0.30	0.452	0.461	0.412	-1.000	0.439	0.456	0.461		0.426	0.520	0.455	-0.768
0.35		0.487	0.449			0.491	0.487	-1.687		0.465	0.470	-1.753
0.40	0.517	0.544	0.104	-2.263	0.485	0.526		-2.095	0.469	0.653		
0.45	0.611	0.734	-0.704		0.617	0.709			0.593	0.715	-16.485	2.333
0.50	0.667		-4.622	-1.874	0.431		-5.125		0.651		-2.653	2.145
0.55		-3.962		0.431		-23.513	-3.199	1.750		-1.550	2.576	
0.60	-3.781	-4.895		0.928	-1.882	-2.023	1.310	1.729	0.818	6.199	2.447	2.664

Table 4

DAMPING DERIVATIVE $-m_{\dot{\theta}}$ FOR NPL 9615 SMOOTH SURFACE

(a) 3^{o} oscillation amplitude

M \ α	67 Hz				58 Hz				43 Hz				
	10	11	12	14	10	11	12	14	10	11	12	14	16
0.30	0.392	0.404	0.421	0.391	0.397	0.390	0.401	0.467	0.431	0.366	0.380	0.428	-0.908
0.35				-0.056				-0.423			0.496	-0.743	-2.159
0.40	0.465	0.531	-0.032	-0.910	0.489	0.567	0.021	-0.857	0.541	0.561	-0.265	-0.710	-0.498
0.45		0.324	-0.345	-1.026		0.147	-0.383	-0.815		-0.005	-0.246	0.045	1.021
0.50	0.230	-0.168	-0.553	-0.750	0.134	-0.162	-0.375	-0.404	0.696	0.016	0.085	1.004	1.753
0.55	0.031	-0.190	-0.270	-0.292	-0.081	-0.152		0.172		0.361	0.528	2.447	
0.60	0.033	-0.098	-0.030	-0.353	0.045	0.168	0.261	1.658	0.689	1.138	1.525	1.869	2.904

(b) 2^{o} oscillation amplitude

0.30	0.448	0.451	0.462	0.416	0.447	0.452	0.460	0.450	0.444	0.464	0.513	0.530	-0.688
0.35				0.412				0.119			0.613	-0.825	-1.967
0.40	0.509	0.568	0.457	-0.998	0.528	0.615	0.541	-1.389	0.594	0.637	0.770	-1.579	-0.822
0.45		0.701	-0.323	-1.454		0.758	-0.405	-1.491		0.784	-0.467	-0.301	1.645
0.50	0.777	0.082	-0.831	-1.351	0.671	-0.271	-0.710	-0.679	0.910	0.033	-0.151	1.136	1.898
0.55	0.268	-0.416	-0.533	-0.501	0.240	-0.316	-0.415	0.251		0.243	0.609	2.568	
0.60	-0.053	-0.246	-0.210	0.367	0.037	0.064	0.390	1.701	0.855	1.196	1.602	1.983	3.033

Table 4

(c) 1^{o} oscillation amplitude

α	67 Hz				58 Hz				43 Hz				
M	10	11	12	14	10	11	12	14	10	11	12	14	16
0.30	0.462	0.493	0.466	0.444	0.486	0.479	0.480	0.489	0.462	0.451	0.483	0.538	-0.607
0.35				0.470				0.600			0.561	0.627	-1.896
0.40	0.512	0.577	0.956		0.541	0.549	0.698	-2.268	0.527	0.594	0.796		-2.169
0.45		0.746	0.728	-2.013		0.812	0.955	-2.937		0.842	0.871	-1.336	3.180
0.50	0.814	0.731		-2.900	0.920			-1.678	0.912	0.894	-0.489	2.486	2.832
0.55		-0.408	-1.561	-1.038	0.847		-0.788	0.885		0.260	1.195	2.638	
0.60	0.883	-0.552	-0.516	0.829	0.092	0.249	0.865	1.747	1.148	1.418	2.087	2.049	3.080

(d) $\frac{1}{2}^{o}$ oscillation amplitude

0.30	0.439	0.467	0.488	0.452	0.474	0.453	0.463	0.469	0.431	0.429	0.468	0.537	-0.566
0.35								0.630			0.530	0.669	-1.860
0.40	0.527	0.580	1.377	0.510	0.505	0.534	0.780		0.476	0.591	0.747		-5.551
0.45		0.781	0.770			0.836	0.979	-6.033		0.868	0.893	-3.450	1.961
0.50	0.846			-2.274	0.946			-4.744	0.922	0.780		1.949	2.032
0.55	0.913	0.764	-7.184	-11.895	1.325		-1.272	3.178		0.854	2.354	1.756	
0.60		-1.702	-1.305	-1.419	0.809	0.232	2.342	0.723	1.652	2.072	2.105	2.077	3.104

Table 5

DAMPING DERIVATIVE $-m_{\dot{\theta}}$ FOR NPL 9615, ROUGHNESS ADDED

(a) 3° oscillation amplitude

M \ α	67 Hz				58 Hz			
	10	11	12	14	10	11	12	14
0.30	0.419	0.406	0.391	0.387	0.430		0.468	0.360
0.35				0.098			0.464	
0.40	0.485	0.567	0.026	-0.665	0.513	0.521		-0.988
0.45			-0.605		0.281		-0.948	
0.50	-0.069	-0.643	-1.001	-1.215		-0.894	-1.115	-0.815
0.55	-0.715	-0.880	-1.146	-1.119	-0.523	-0.752	-0.997	-0.744
0.60	-0.542	-0.874	-1.134	-0.715	-0.442	-0.570	-0.688	-0.189

(b) 2° oscillation amplitude

0.30	0.465	0.475	0.453	0.363	0.429		0.463	0.383
0.35				0.353			0.488	
0.40	0.536	0.555	0.737	-0.454	0.492	0.534	0.516	-0.756
0.45					0.572	0.225	-0.858	
0.50	0.450	-0.573	-1.405	-1.994		-1.435	-1.833	-0.563
0.55	-0.675	-1.363	-1.790	-2.017	-0.612	-1.277	-1.941	-1.379
0.60	-0.895	-1.457	-1.630		-0.784	-1.269	-1.204	-0.449

(c) 1° oscillation amplitude

0.30	0.475	0.487	0.465	0.377	0.474		0.463	0.373
0.35				0.326			0.527	0.204
0.40	0.526	0.554	0.542	-1.134	0.527	0.566	0.558	-0.556
0.45		0.680	0.161		0.604	0.650		
0.50	0.686		-0.882	-2.558	0.676	-2.598	-1.805	-0.444
0.55		-2.021	-3.251	-2.654		-2.350	-3.883	-1.698
0.60	-4.650	-3.278	-4.089	0.624	-1.813	-2.270	-2.523	

(d) $\frac{1}{2}^{\circ}$ oscillation amplitude

0.30	0.443	0.483	0.447	0.384	0.334		0.452	0.370
0.35				0.328			0.545	0.348
0.40	0.506		0.520	-1.103	0.511	0.583	0.574	-1.264
0.45		0.699	0.738		0.624	0.570		
0.50	0.704		-1.017	-1.427	0.694	-6.989	-1.791	-0.855
0.55		-2.358	-6.028	-3.090		-9.653	-6.588	
0.60	-5.709	-9.672	-4.437	2.180	-8.596	-5.624	-5.140	2.968

Table 5 (concluded)

(a) 3° oscillation amplitude

α / M	43 Hz				36 Hz			
	10	11	12	14	10	11	12	14
0.30	0.271	0.328	0.386		0.475	0.462	0.537	-0.641
0.35			0.473	-1.147		0.494		-1.416
0.40	0.368	0.281		-1.650	0.564	0.471		-2.228
0.45	0.189	-0.877	-1.055	-1.374		-0.554	-0.818	-0.225
0.50		-0.733	-0.544	-0.061		-0.332	-0.119	
0.55	-0.318	-0.168	0.343		-0.092	0.208	0.529	
0.60	0.073		1.045	1.205	0.428	1.415	1.873	3.171

(b) 2° oscillation amplitude

0.30	0.431	0.459	0.458	0.329	0.456	0.472	0.509	0.190
0.35			0.501			0.503	0.540	-1.409
0.40	0.519	0.543	-0.736	-2.064	0.523	0.555		-2.222
0.45	0.592		-2.200	-1.889	0.409		-0.807	-1.102
0.50	0.658	-1.286	-1.394		0.683	-0.949	-0.648	-0.033
0.55	-0.957	-0.649	-0.241		-0.074	-0.134	0.363	
0.60	0.019	0.474	1.086	1.826	0.435	1.421	1.882	3.176

(c) 1° oscillation amplitude

0.30	0.454	0.497	0.479	0.377	0.463	0.490	0.503	0.463
0.35			0.535	-0.038		0.519	0.553	
0.40	0.478	0.545	0.608	-2.210	0.504	0.563	0.700	-2.208
0.45	0.569	0.639		-3.634	0.672	0.690		-1.384
0.50	0.713		-3.418		0.697			0.472
0.55		-1.822	-1.830		0.787	-1.712	0.288	
0.60	-0.273	0.624	1.138	2.097	0.447	1.431	1.890	3.185

(d) $\frac{1}{2}^{\circ}$ oscillation amplitude

0.30	0.452	0.479	0.476	0.392	0.449	0.496	0.479	0.472
0.35			0.516	0.207		0.523	0.562	
0.40	0.459	0.510	0.574	-4.446	0.468	0.567	0.602	-2.200
0.45	0.559	0.664		-5.211	1.062	0.694		-1.954
0.50	0.719		-15.185		0.702			2.135
0.55		-5.638	-11.268		0.792		-0.689	
0.60	-1.392	0.811	1.153	2.690	0.451	1.434	1.895	3.191

Table 5

DAMPING DERIVATIVE $-m_{\dot{\theta}}$ FOR NPL 9615, ROUGHNESS ADDED

(a) 3^{o} oscillation amplitude

α / M	67 Hz				58 Hz			
	10	11	12	14	10	11	12	14
0.30	0.419	0.406	0.391	0.387	0.430		0.468	0.360
0.35				0.098			0.464	
0.40	0.485	0.567	0.026	-0.665	0.513	0.521		-0.988
0.45			-0.605		0.281		-0.948	
0.50	-0.069	-0.643	-1.001	-1.215		-0.894	-1.115	-0.815
0.55	-0.715	-0.880	-1.146	-1.119	-0.523	-0.752	-0.997	-0.744
0.60	-0.542	-0.874	-1.134	-0.715	-0.442	-0.570	-0.688	-0.189

(b) 2^{o} oscillation amplitude

0.30	0.465	0.475	0.453	0.363	0.429		0.463	0.383
0.35				0.353			0.488	
0.40	0.536	0.555	0.737	-0.454	0.492	0.534	0.516	-0.756
0.45					0.572	0.225	-0.858	
0.50	0.450	-0.573	-1.405	-1.994		-1.435	-1.833	-0.563
0.55	-0.675	-1.363	-1.790	-2.017	-0.612	-1.277	-1.941	-1.379
0.60	-0.895	-1.457	-1.630		-0.784	-1.269	-1.204	-0.449

(c) 1^{o} oscillation amplitude

0.30	0.475	0.487	0.465	0.377	0.474		0.463	0.373
0.35				0.326			0.527	0.204
0.40	0.526	0.554	0.542	-1.134	0.527	0.566	0.558	-0.556
0.45		0.680	0.161		0.604	0.650		
0.50	0.686		-0.882	-2.558	0.676	-2.598	-1.805	-0.444
0.55		-2.021	-3.251	-2.654		-2.350	-3.883	-1.698
0.60	-4.650	-3.278	-4.089	0.624	-1.813	-2.270	-2.523	

(d) $\frac{1}{2}^{o}$ oscillation amplitude

0.30	0.443	0.483	0.447	0.384	0.334		0.452	0.370
0.35				0.328			0.545	0.348
0.40	0.506		0.520	-1.103	0.511	0.583	0.574	-1.264
0.45		0.699	0.738		0.624	0.570		
0.50	0.704		-1.017	-1.427	0.694	-6.989	-1.791	-0.855
0.55		-2.358	-6.028	-3.090		-9.653	-6.588	
0.60	-5.709	-9.672	-4.437	2.180	-8.596	-5.624	-5.140	2.968

Table 5 (concluded)

(a) 3° oscillation amplitude

M \ α	43 Hz				36 Hz			
	10	11	12	14	10	11	12	14
0.30	0.271	0.328	0.386		0.475	0.462	0.537	-0.641
0.35			0.473	-1.147		0.494		-1.416
0.40	0.368	0.281		-1.650	0.564	0.471		-2.228
0.45	0.189	-0.877	-1.055	-1.374		-0.554	-0.818	-0.225
0.50		-0.733	-0.544	-0.061		-0.332	-0.119	
0.55	-0.318	-0.168	0.343		-0.092	0.208	0.529	
0.60	0.073		1.045	1.205	0.428	1.415	1.873	3.171

(b) 2° oscillation amplitude

0.30	0.431	0.459	0.458	0.329	0.456	0.472	0.509	0.190
0.35			0.501			0.503	0.540	-1.409
0.40	0.519	0.543	-0.736	-2.064	0.523	0.555		-2.222
0.45	0.592		-2.200	-1.889	0.409		-0.807	-1.102
0.50	0.658	-1.286	-1.394		0.683	-0.949	-0.648	-0.033
0.55	-0.957	-0.649	-0.241		-0.074	-0.134	0.363	
0.60	0.019	0.474	1.086	1.826	0.435	1.421	1.882	3.176

(c) 1° oscillation amplitude

0.30	0.454	0.497	0.479	0.377	0.463	0.490	0.503	0.463
0.35			0.535	-0.038		0.519	0.553	
0.40	0.478	0.545	0.608	-2.210	0.504	0.563	0.700	-2.208
0.45	0.569	0.639		-3.634	0.672	0.690		-1.384
0.50	0.713		-3.418		0.697			0.472
0.55		-1.822	-1.830		0.787	-1.712	0.288	
0.60	-0.273	0.624	1.138	2.097	0.447	1.431	1.890	3.185

(d) $\frac{1}{2}^{\circ}$ oscillation amplitude

0.30	0.452	0.479	0.476	0.392	0.449	0.496	0.479	0.472
0.35			0.516	0.207		0.523	0.562	
0.40	0.459	0.510	0.574	-4.446	0.468	0.567	0.602	-2.200
0.45	0.559	0.664		-5.211	1.062	0.694		-1.954
0.50	0.719		-15.185		0.702			2.135
0.55		-5.638	-11.268		0.792		-0.689	
0.60	-1.392	0.811	1.153	2.690	0.451	1.434	1.895	3.191

SYMBOLS

C_{Lmax}	maximum value of the steady lift coefficient
$\bar{C}_m$	(complex pitching moment)/qc^2s
c	model chord
f	frequency of oscillation
M	Mach number
m_θ, $m_{\dot{\theta}}$	nondimensional pitching-moment derivatives defined in equation (1)
q	dynamic pressure
s	modal span
V	tunnel speed
α	mean incidence (degrees)
θ	pitching amplitude (degrees)
θ_0	initial displacement (degrees)
ν	frequency parameter = $\omega c/V$
ω	$2\pi f$

REFERENCES

No.	Author(s)	Title, etc.
1	N. Gregory P.G. Wilby	NPL 9615 and NACA 0012 - a comparison of aerodynamic data. ARC CP No.1261 (1968)
2	J. Liiva L. Gray	Two-dimensional tests on airfoils oscillating near stall. Data Report USAAVLABS TR-68 13 B, Vol.II (1968)
3	J. Liiva F.J. Davenport	Dynamic stall of airfoil sections for high-speed rotors. American Helicopter Society Twenty-fourth Annual National Forum Proceedings, May 1968
4	J. Liiva	Unsteady aerodynamic and stall effects on helicopter rotor blade airfoil sections. J. Aircraft, Vol.6, No.1 (1969)
5	K.C. Wight	Oscillatory rigs at the NPL for the measurement of aerodynamic derivatives. NPL Aero Note 1066 (ARC 29987) (1968)
6	K.C. Wight Miss J.A. Nixon	Measurements of the direct oscillatory derivatives for a linear bending mode on four rigid half-span models at subsonic and transonic speeds, in closed and slotted tunnels. ARC R&M 3376 (1963)
7	P.G. Wilby V.G. Quincey	Some effects due to different carborundum bands on the leading edges of aerofoils at high incidence in a subsonic free stream. NPL Aero Note 1081 (ARC 31177) (1969)
8	J.B. Bratt	Wind-tunnel techniques for the measurement of oscillatory derivatives. ARC R&M 3319 (1960)
9	G.F. Moss P.M. Murdin	Two-dimensional low-speed tunnel tests on the NACA 0012 section including measurements made during pitching oscillations at the stall. ARC CP No.1145 (1968)

REFERENCES (Concluded)

No.	Author(s)	Title, etc.
10	A.W. Moore K.C. Wight	On achieving interference-free results from dynamic tests on half-models in transonic wind tunnels. ARC R&M 3636 (1969)
11	J. Osborne	Private communication, July 1970

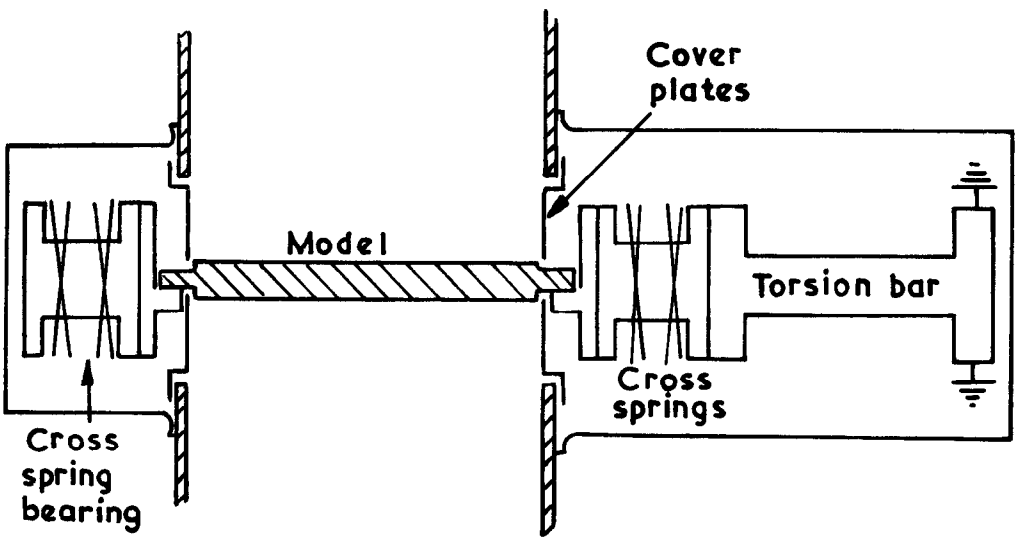

Fig.1 Schematic diagram of oscillating rig

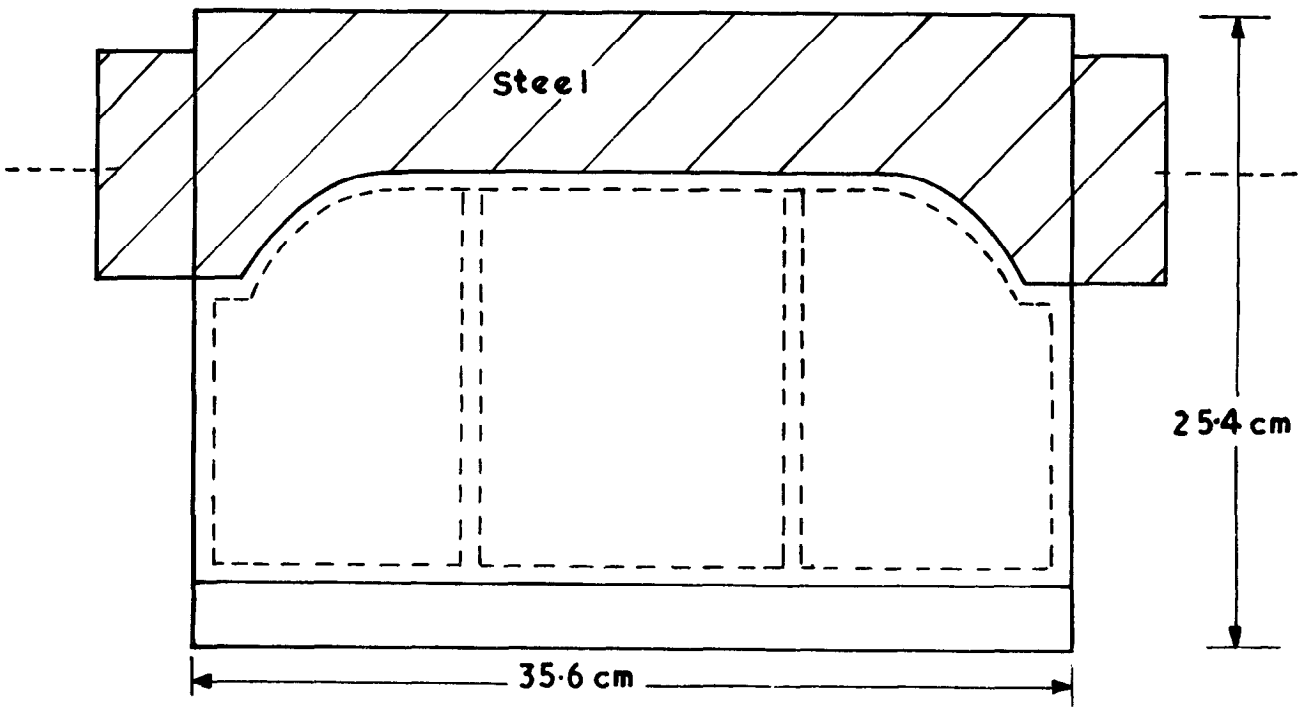

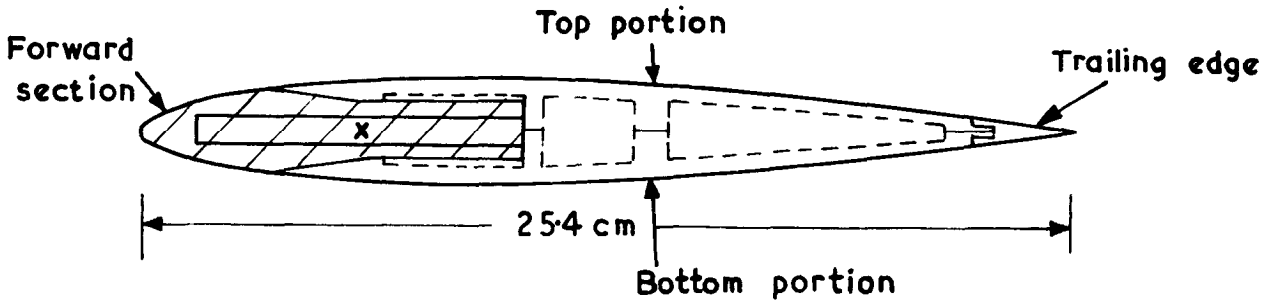

Fig.2 NACA 0012 mass-balanced about one-quarter chord

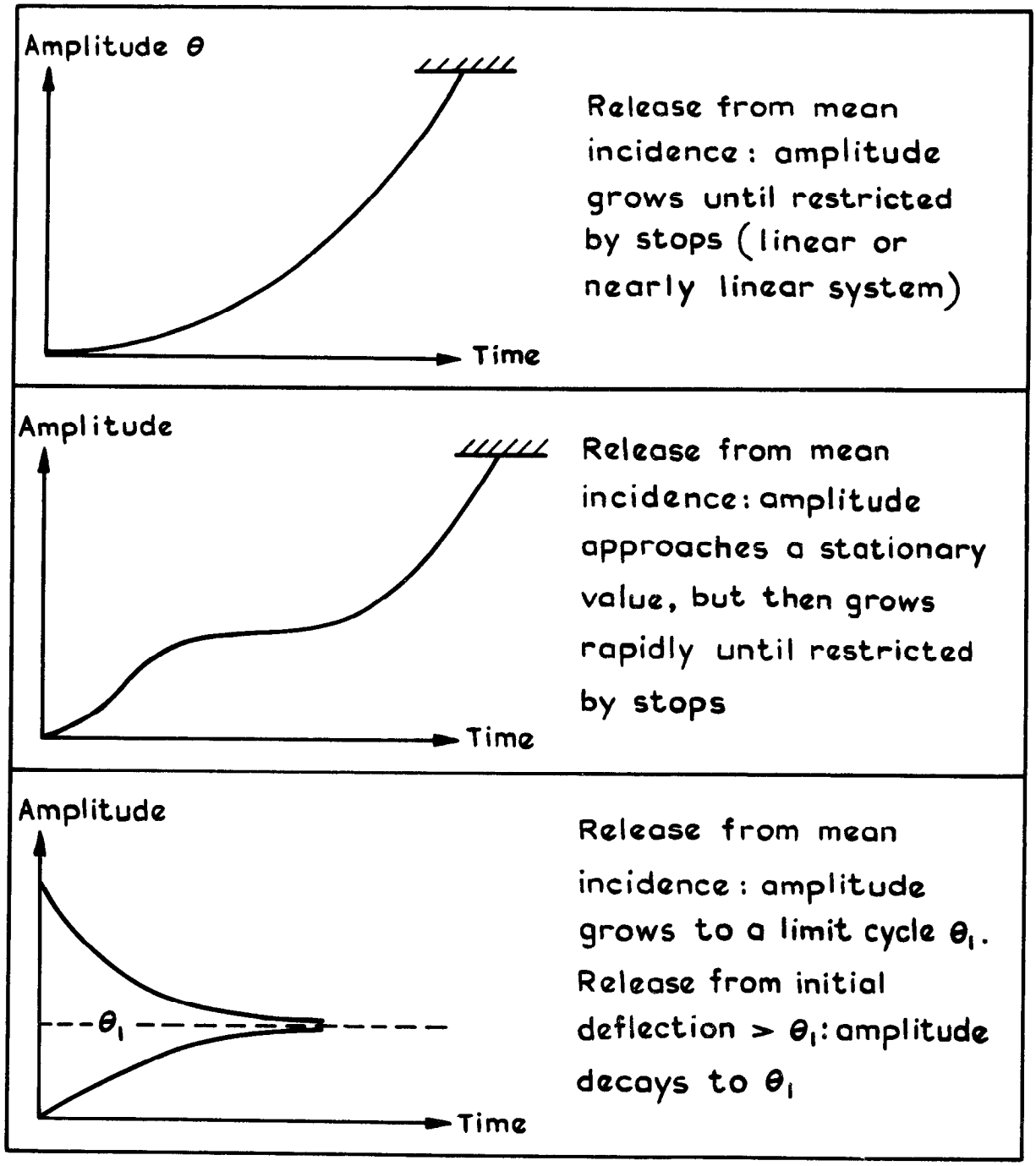

Fig.3a Examples of transient behaviour encountered with different combinations of M and α

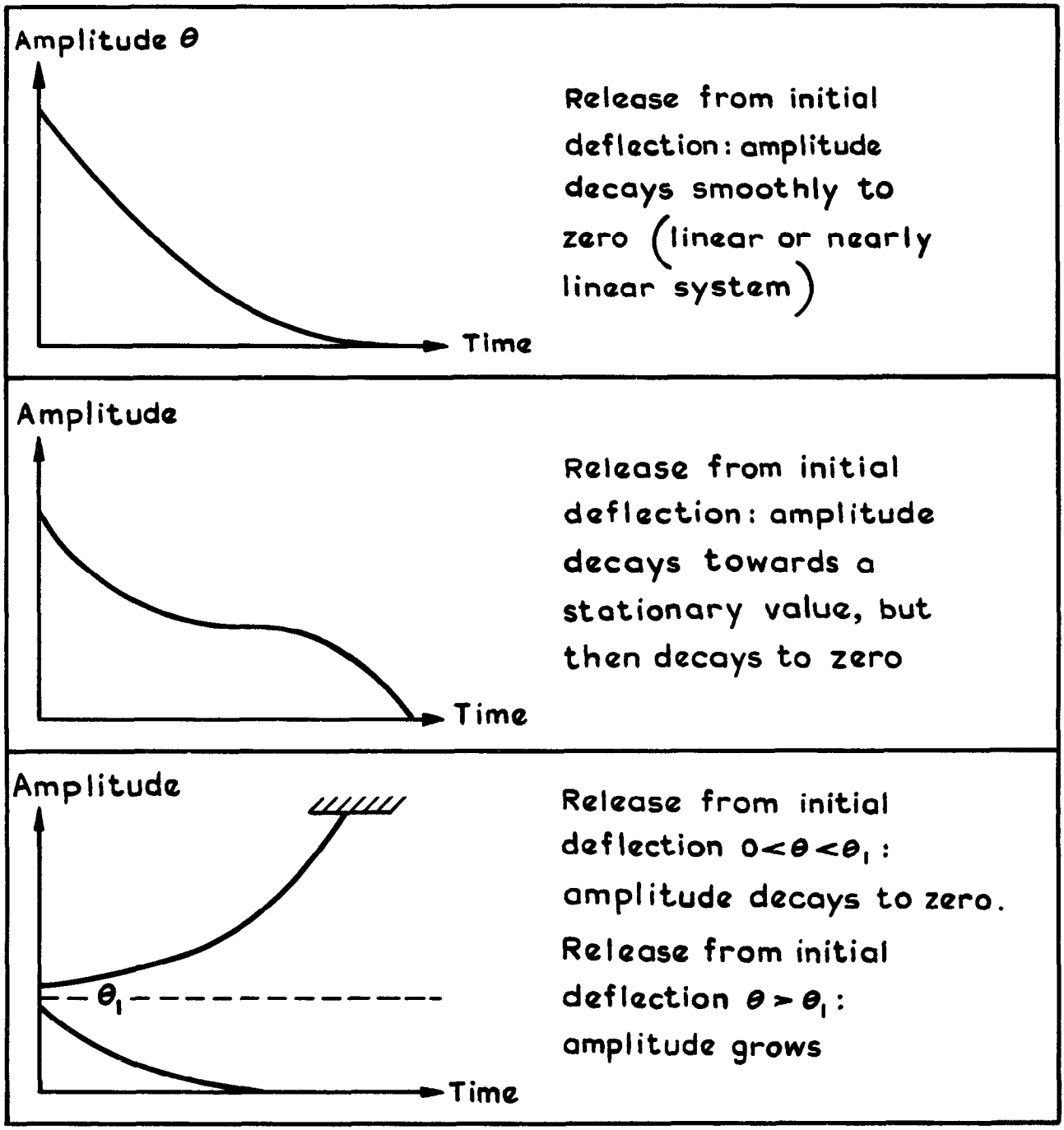

Fig.3b Examples of transient behaviour encountered with different combinations of M and α

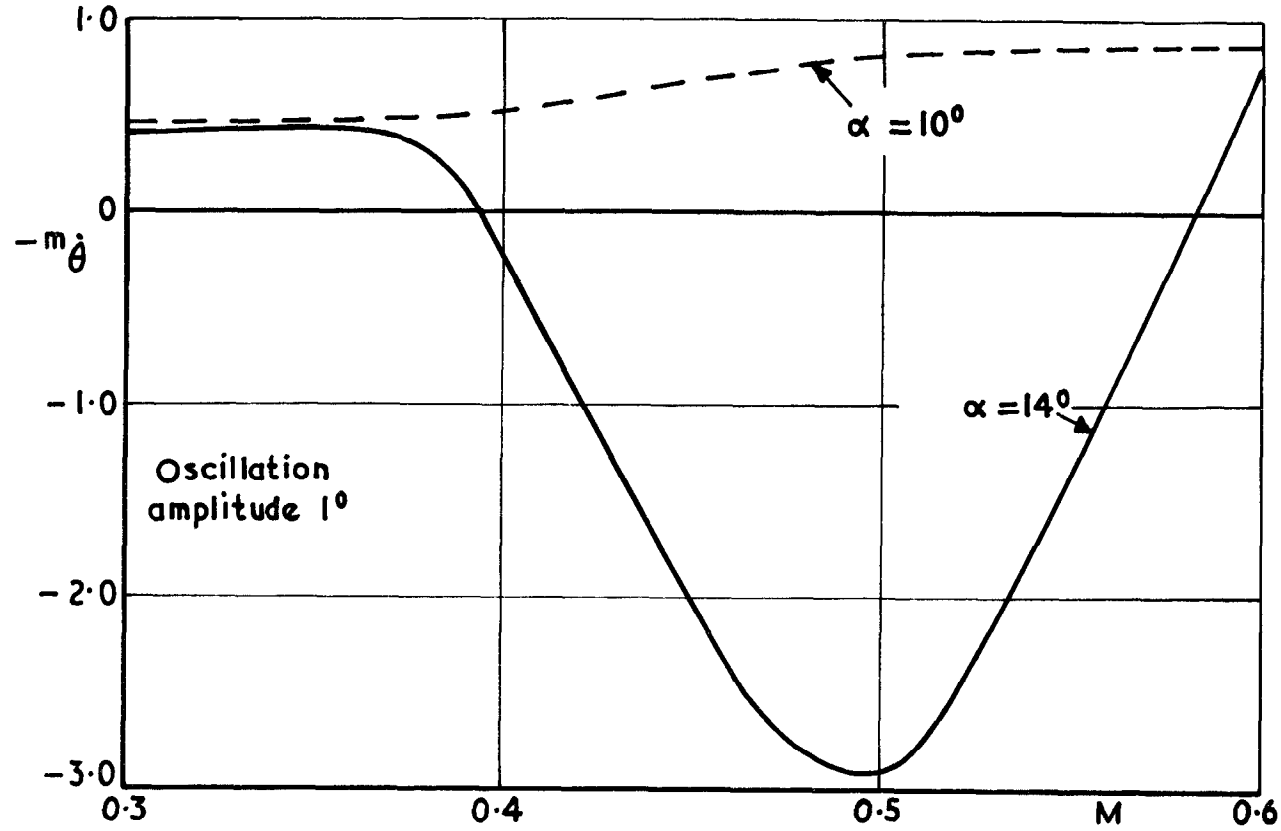

Fig.4 Pitching damping for NPL 9615 with smooth surface, 67 Hz

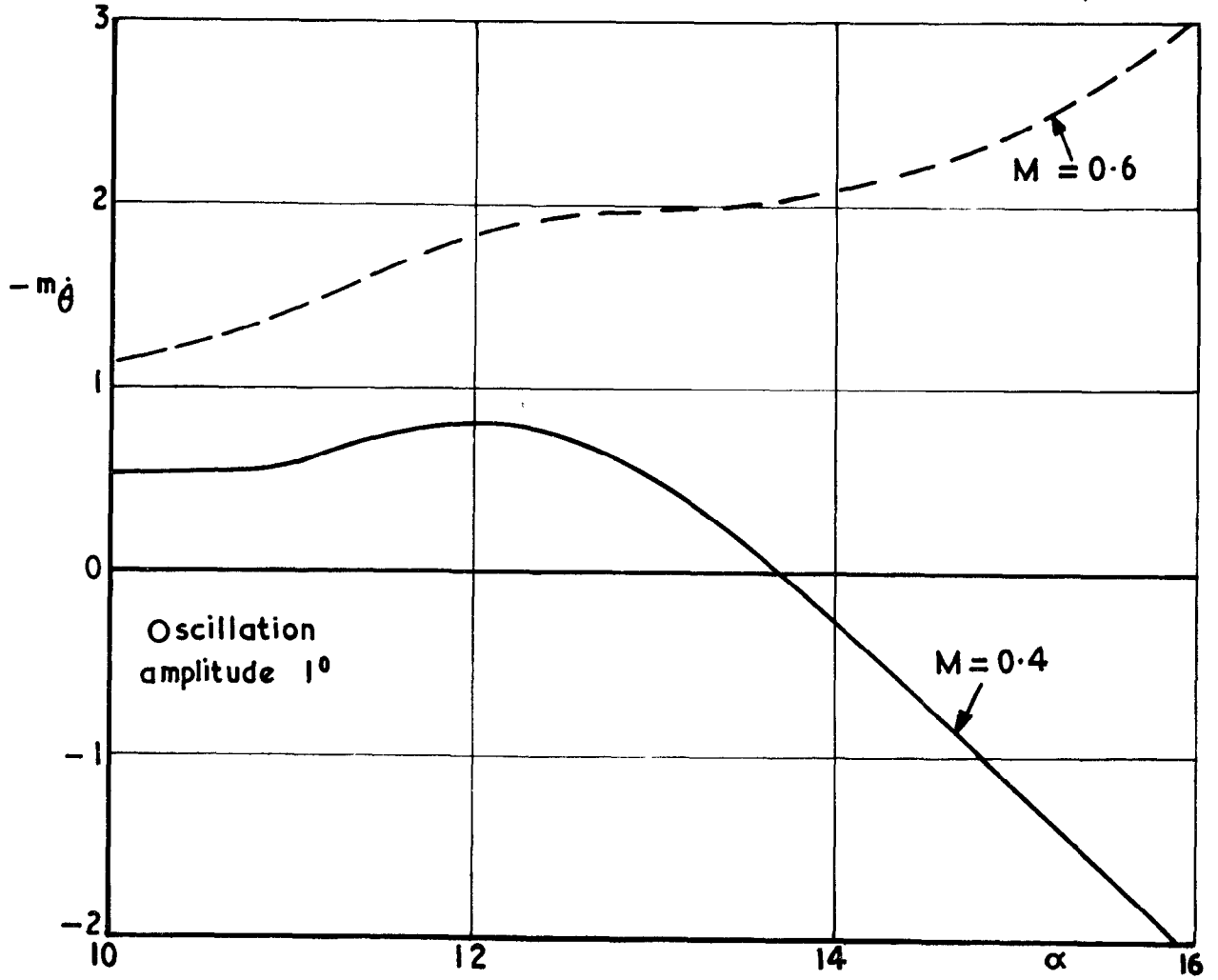

Fig.5 Pitching damping for NPL 9615 with smooth surface, 43 Hz

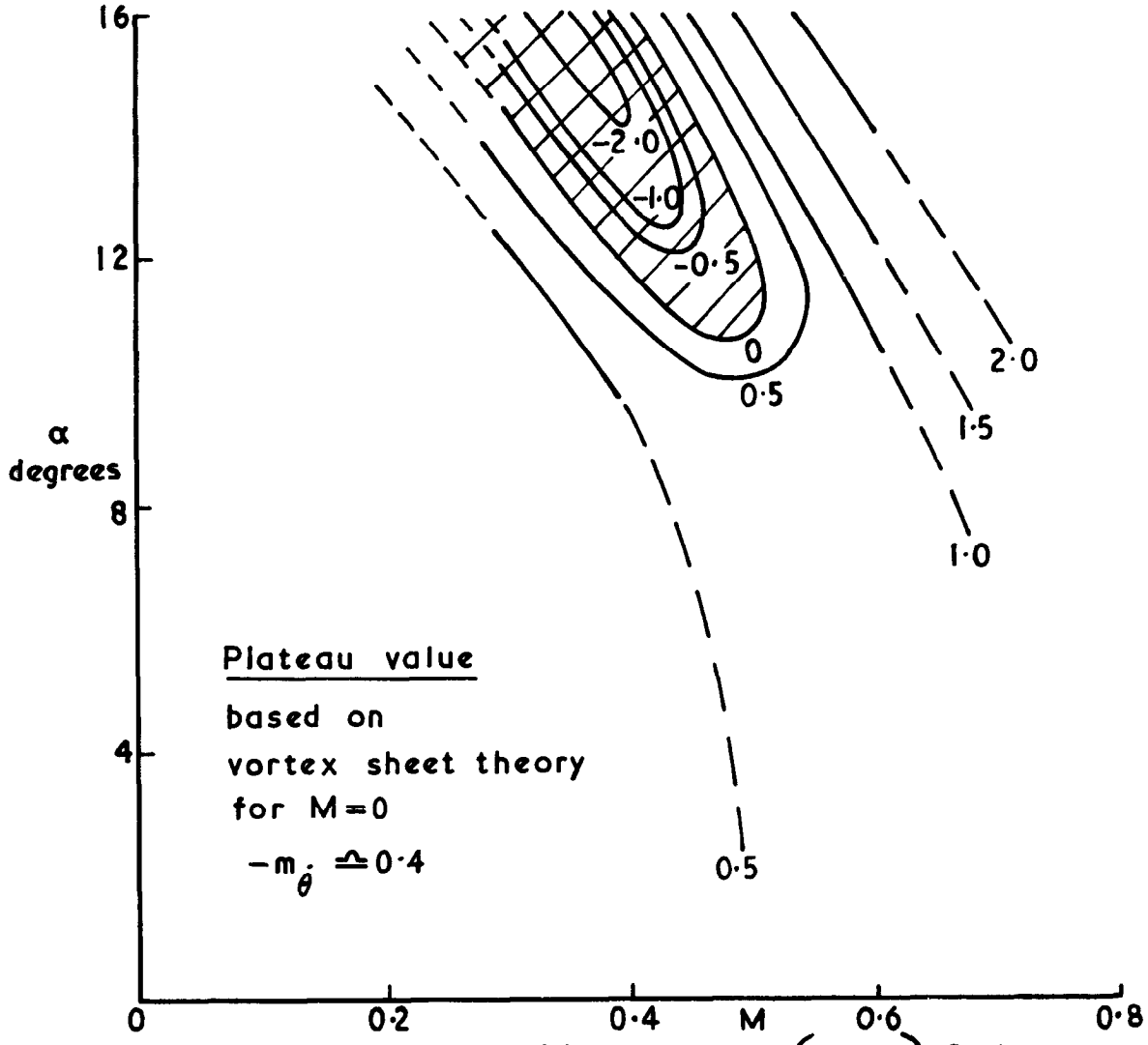

Fig.6 Contours of pitching damping $(-m_{\dot{\theta}})$. Schematic only

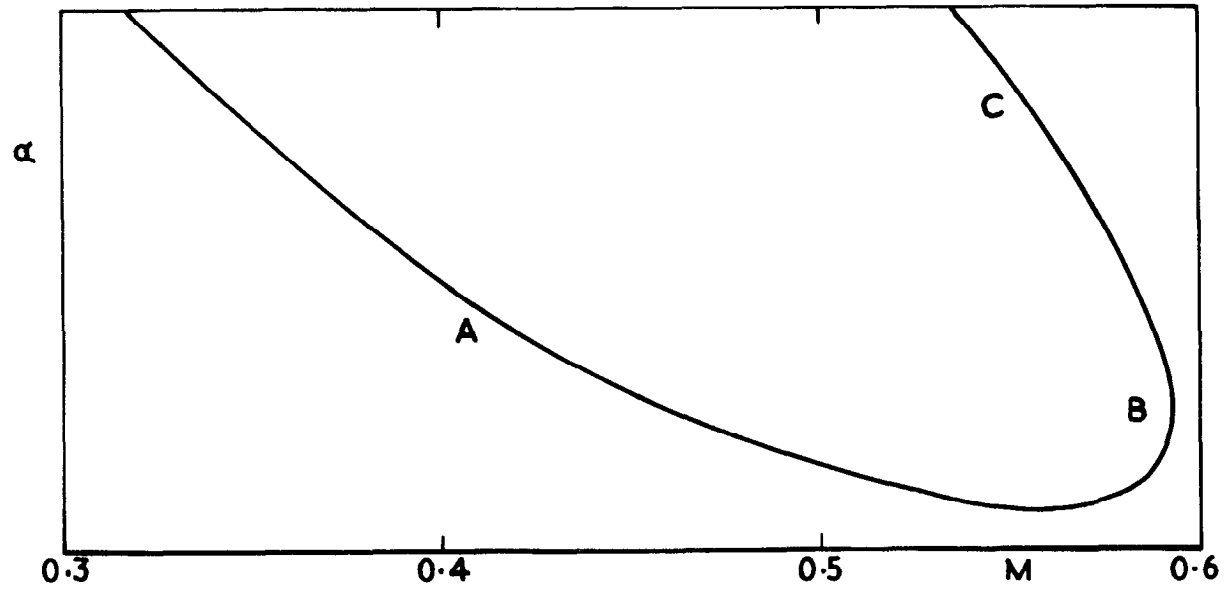

Fig.7 General form of loci of zero damping

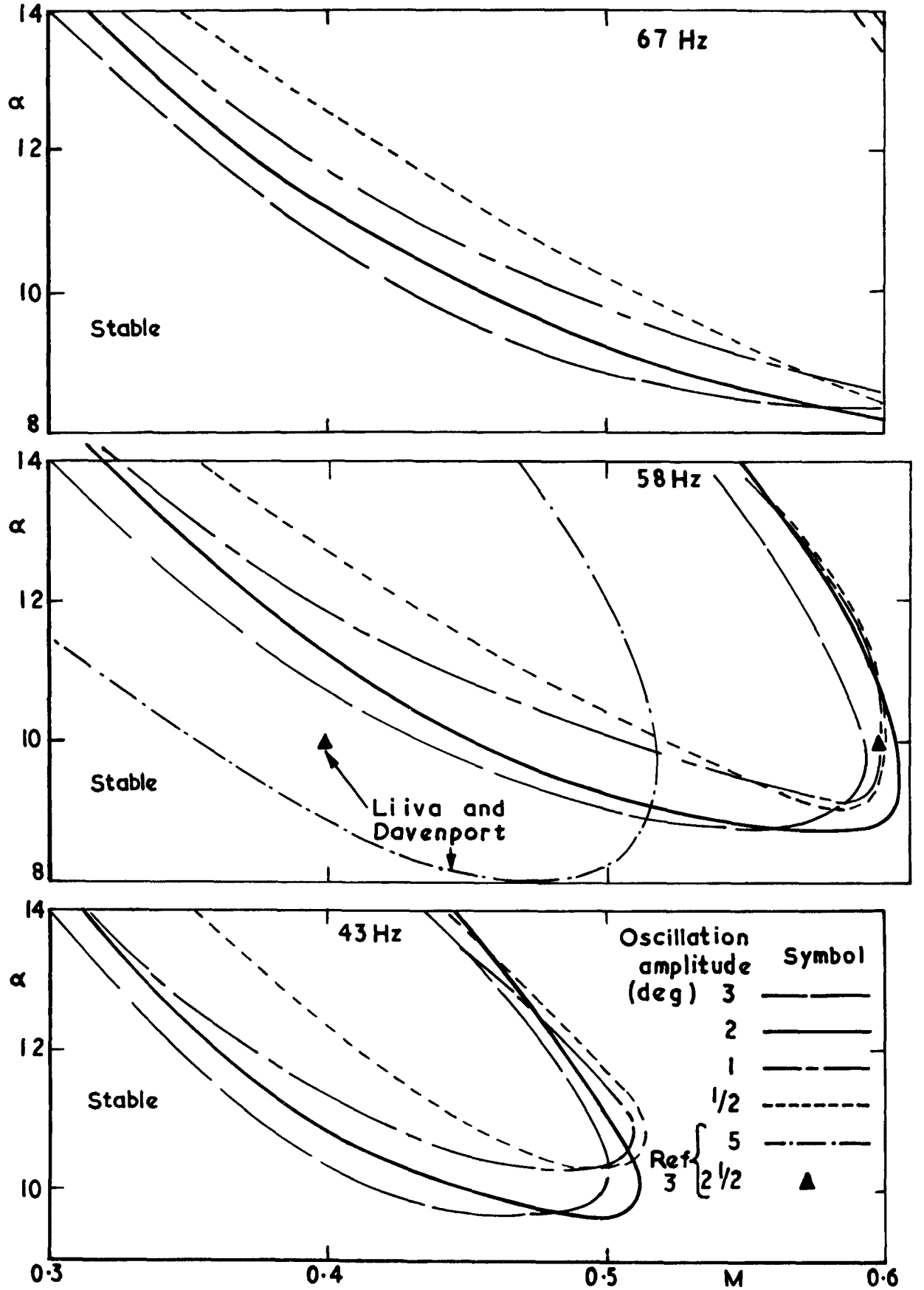

Fig.8 Stability boundaries for NACA 0012 showing the effect of oscillation amplitude; smooth surface

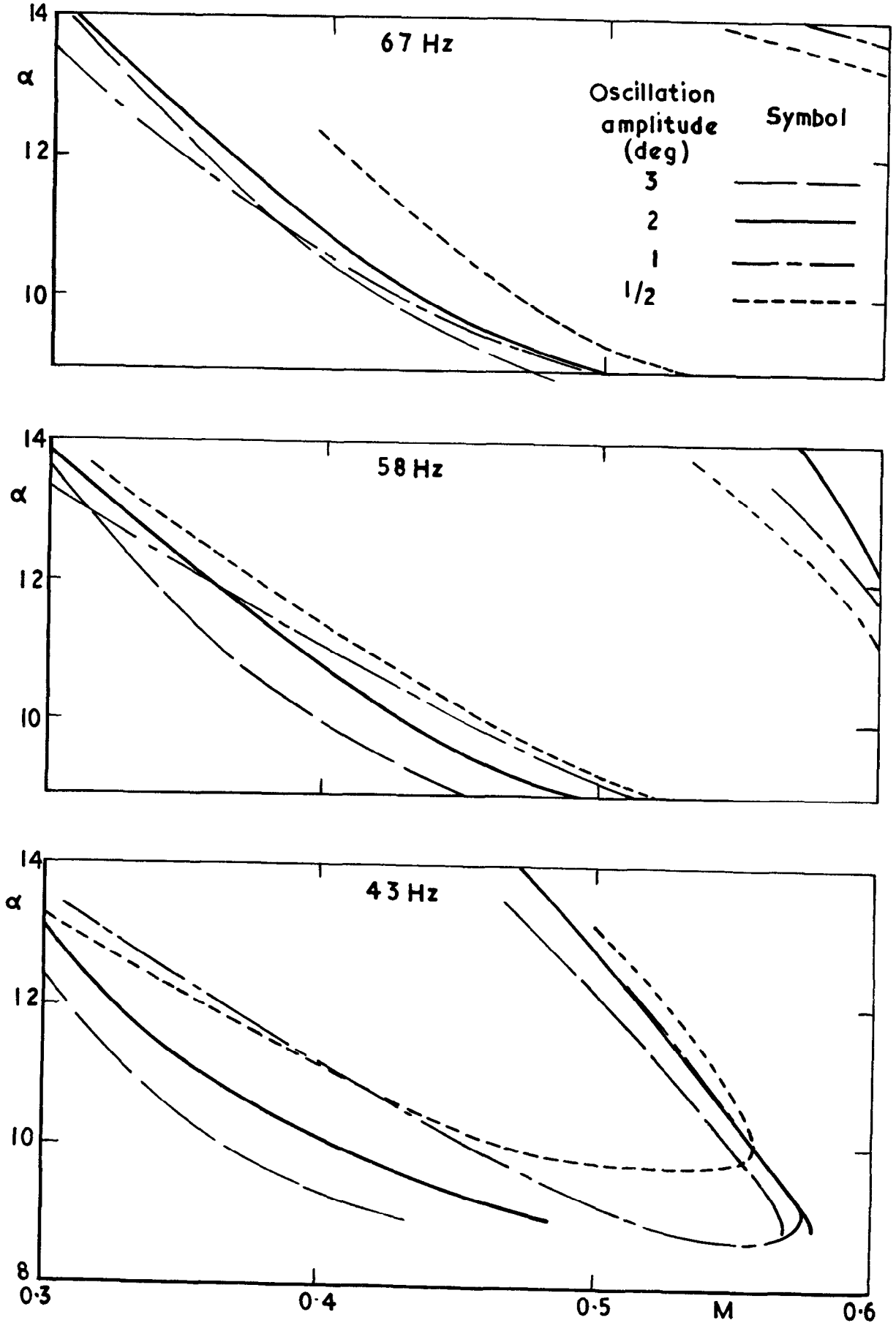

Fig.9 Stability boundaries for NACA 0012 showing the effect of oscillation amplitude; roughness added

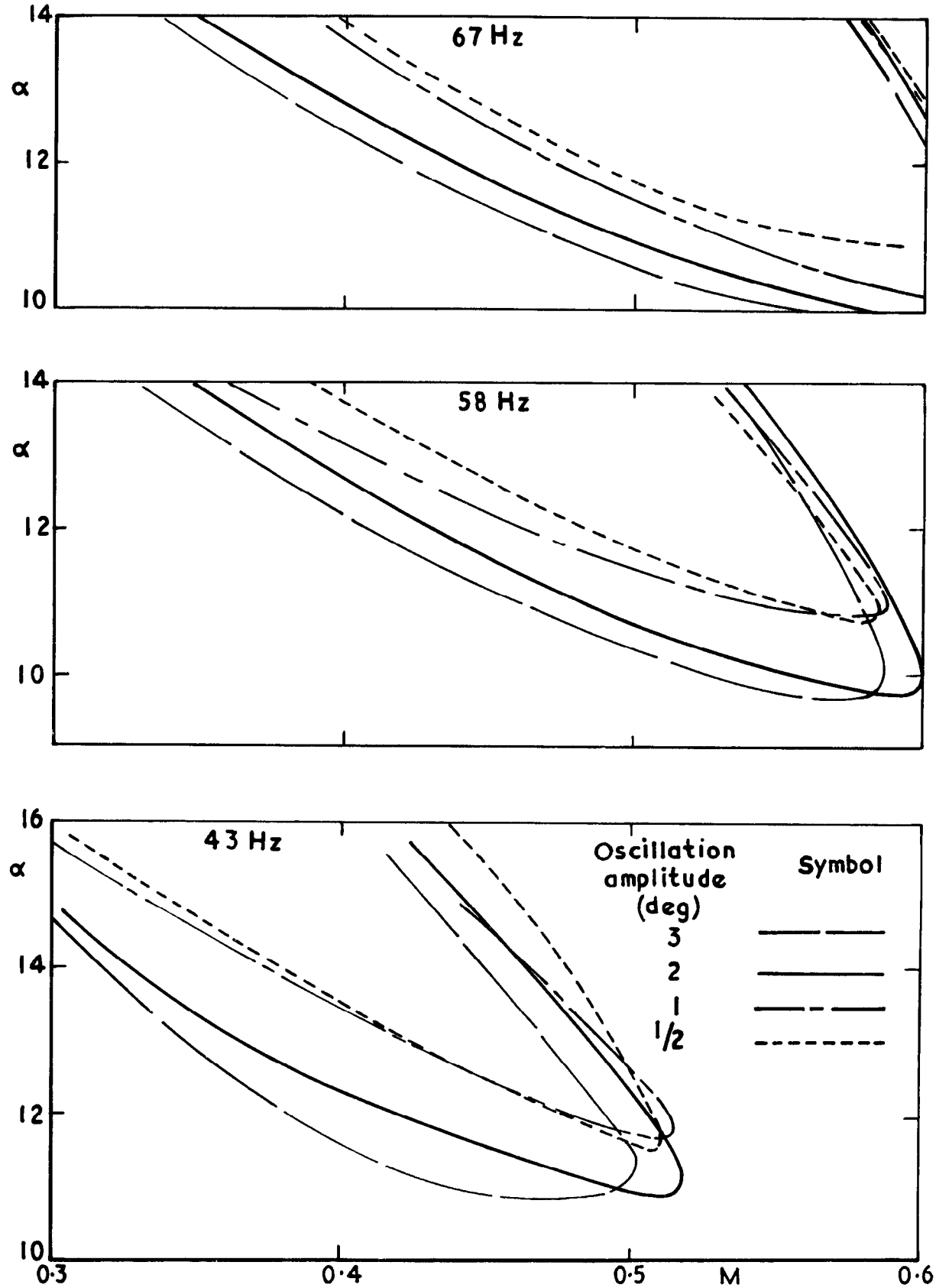

Fig.10 Stability boundaries for NPL 9615 showing the effect of oscillation amplitude; smooth surface

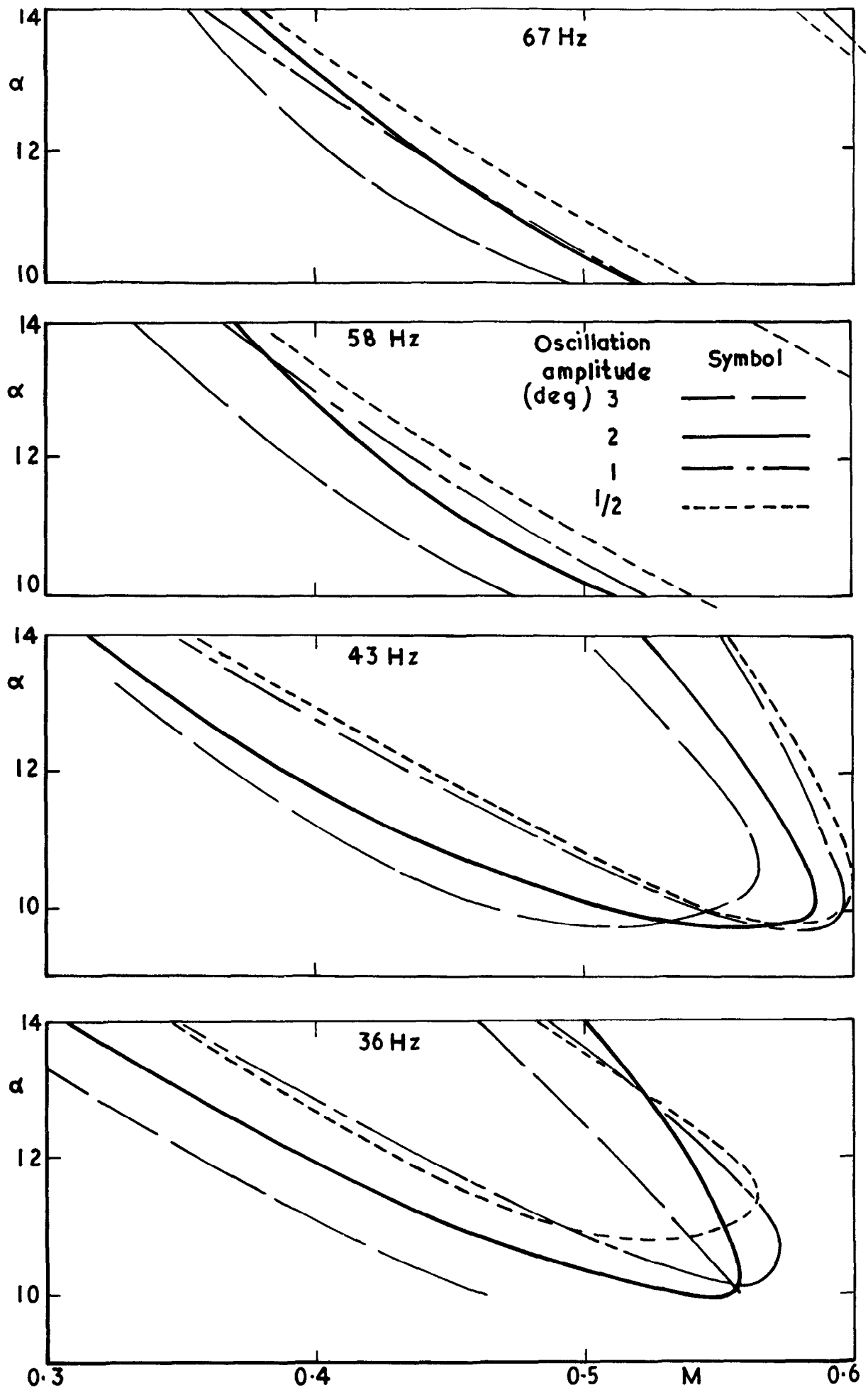

Fig.11 Stability boundaries for NPL 9615 showing the effect of oscillation amplitude; roughness added

Symbol	Frequency	ωc / V
———	67 Hz	0·55 → 1·07
— — —	58 Hz	0·46 → 0·92
- - - - -	43 Hz	0·35 → 0·69

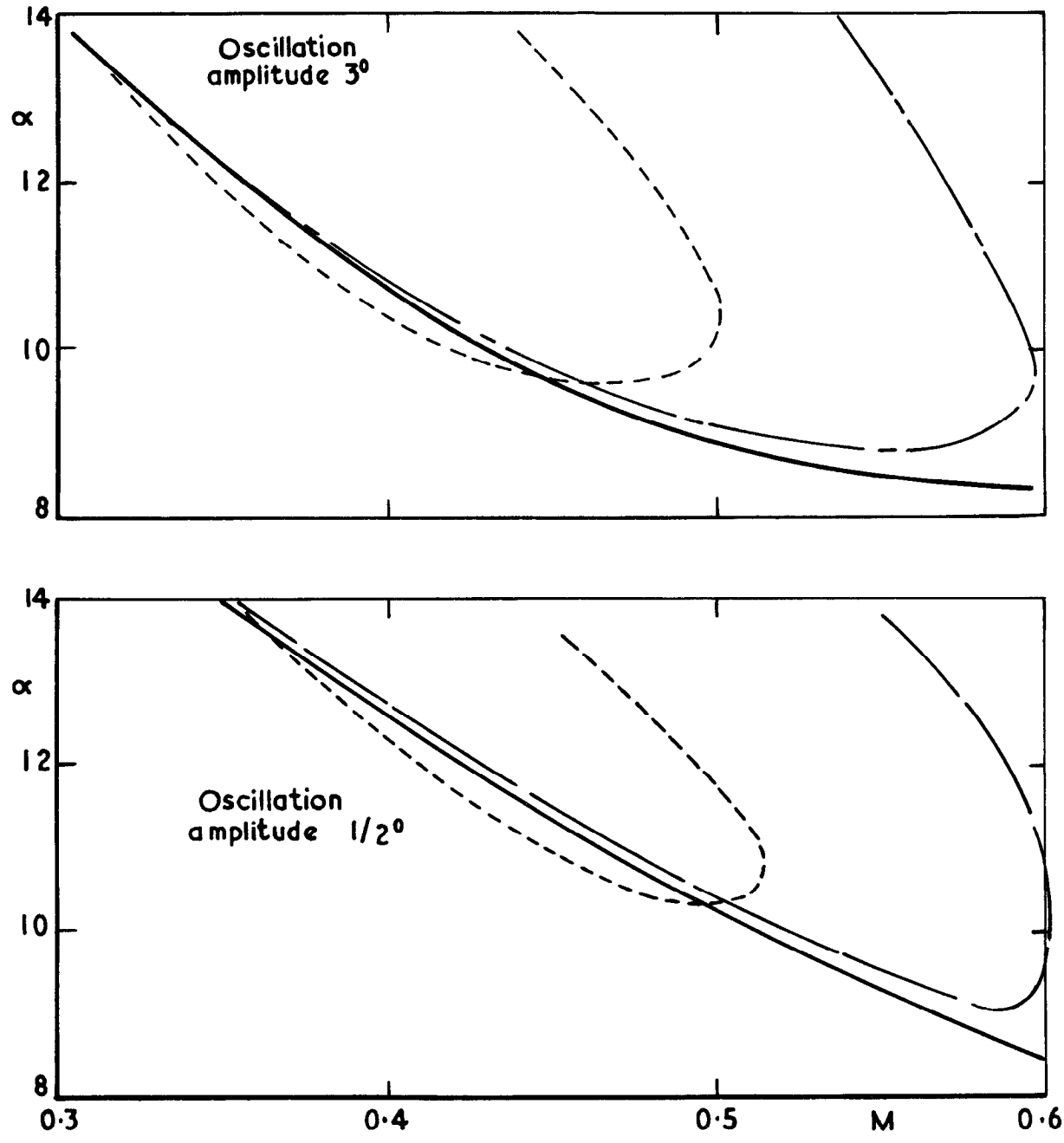

Fig.12 Effect of frequency: NACA 0012 with smooth surface

Symbol	Frequency	ωc / V
———	67 Hz	0·55 → 1·07
— —	58 Hz	0·46 → 0·92
- - - - -	43 Hz	0·35 → 0·69

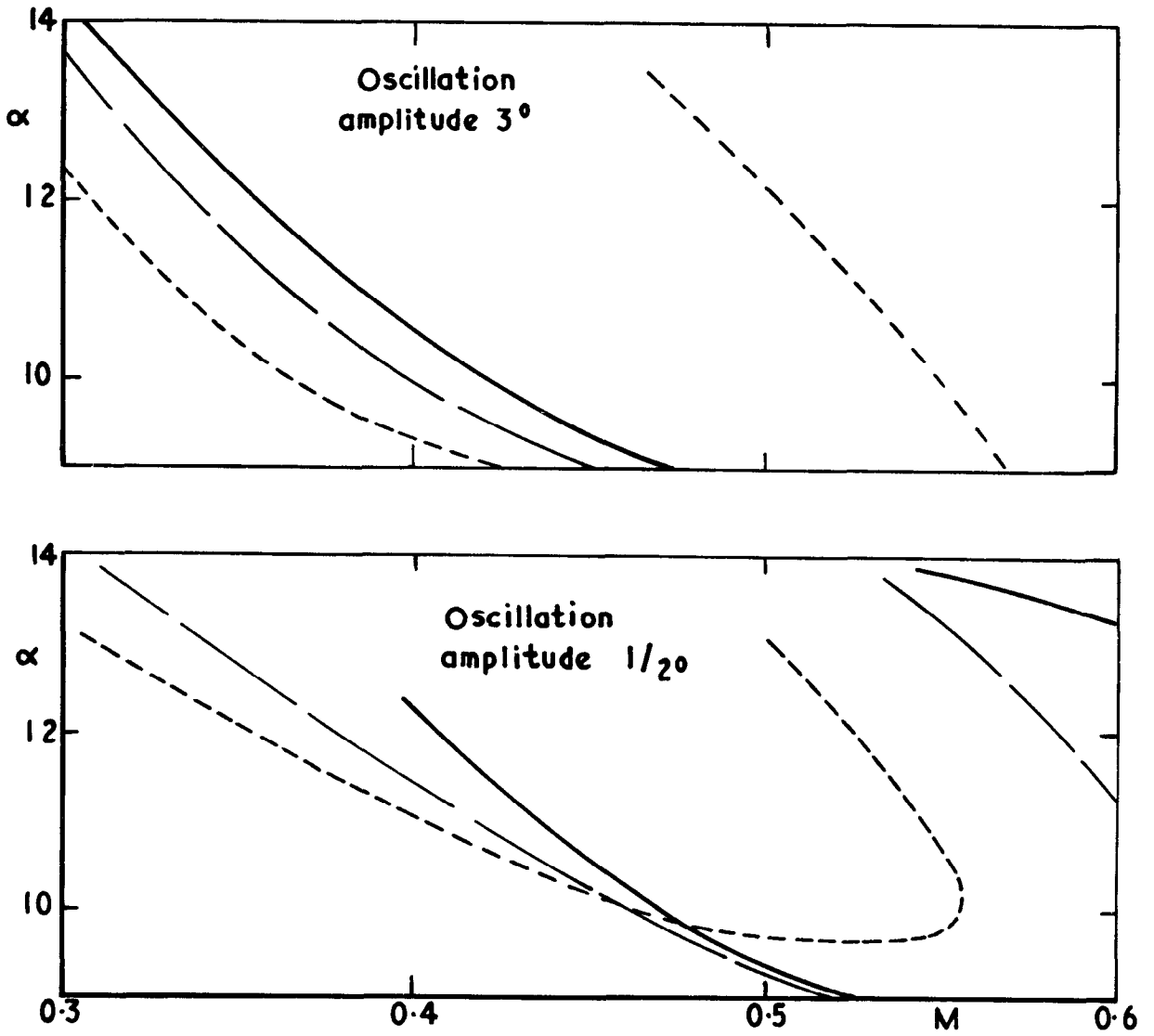

Fig.13 Effect of frequency; NACA 0012 with roughness added

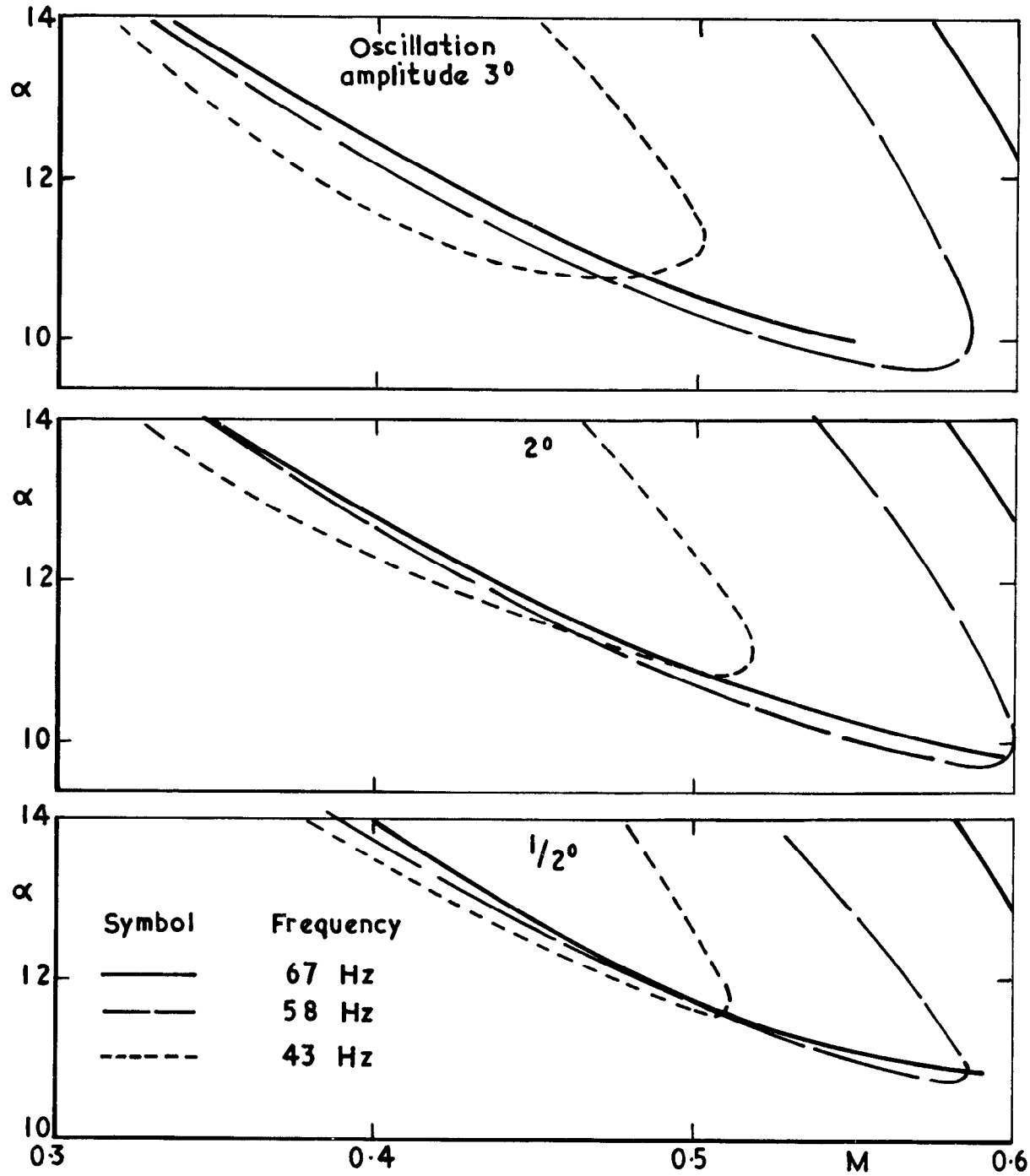

Fig.14 Effect of frequency; NPL 9615 with smooth surface

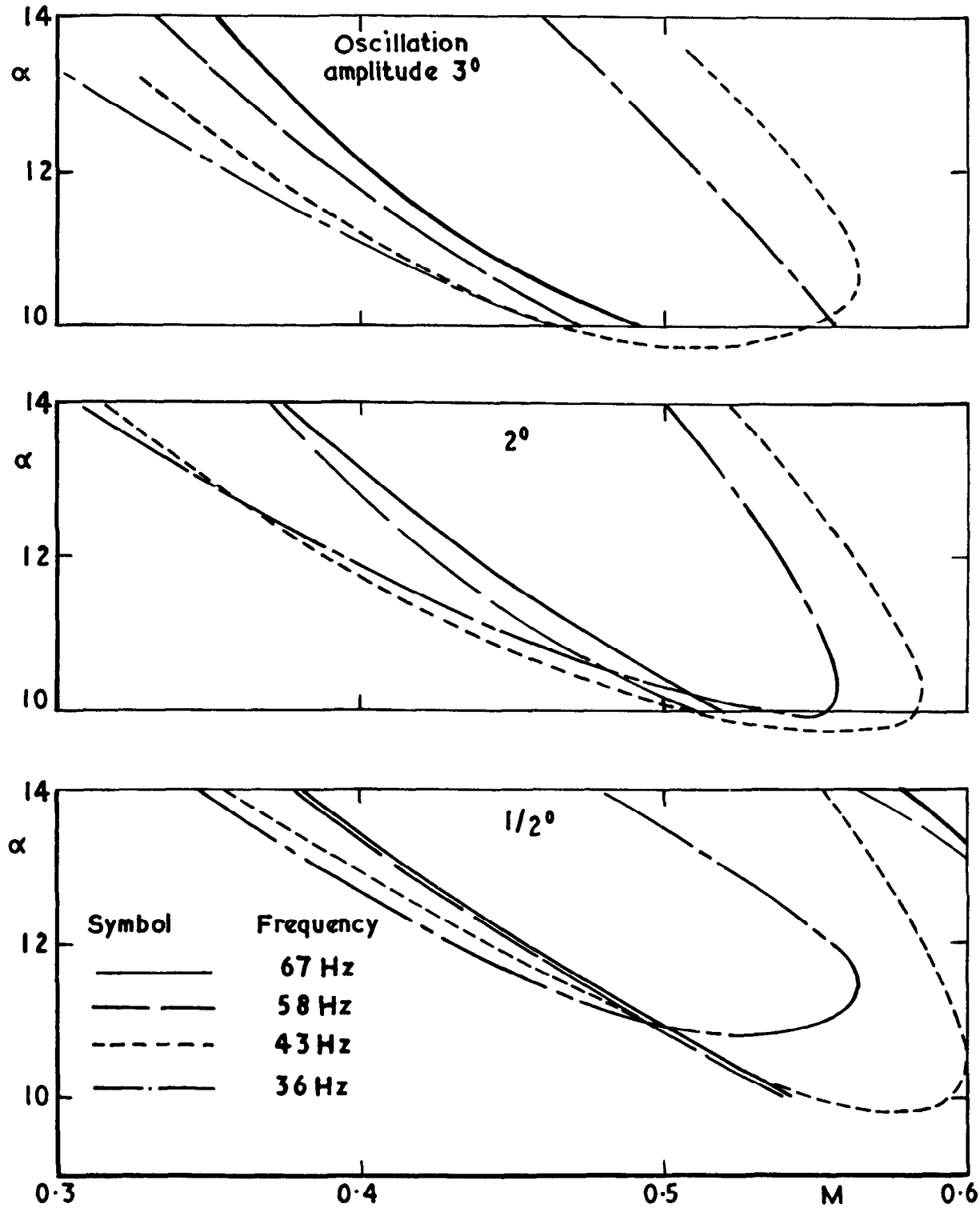

Fig.15 Effect of frequency; NPL 9615 with roughness added

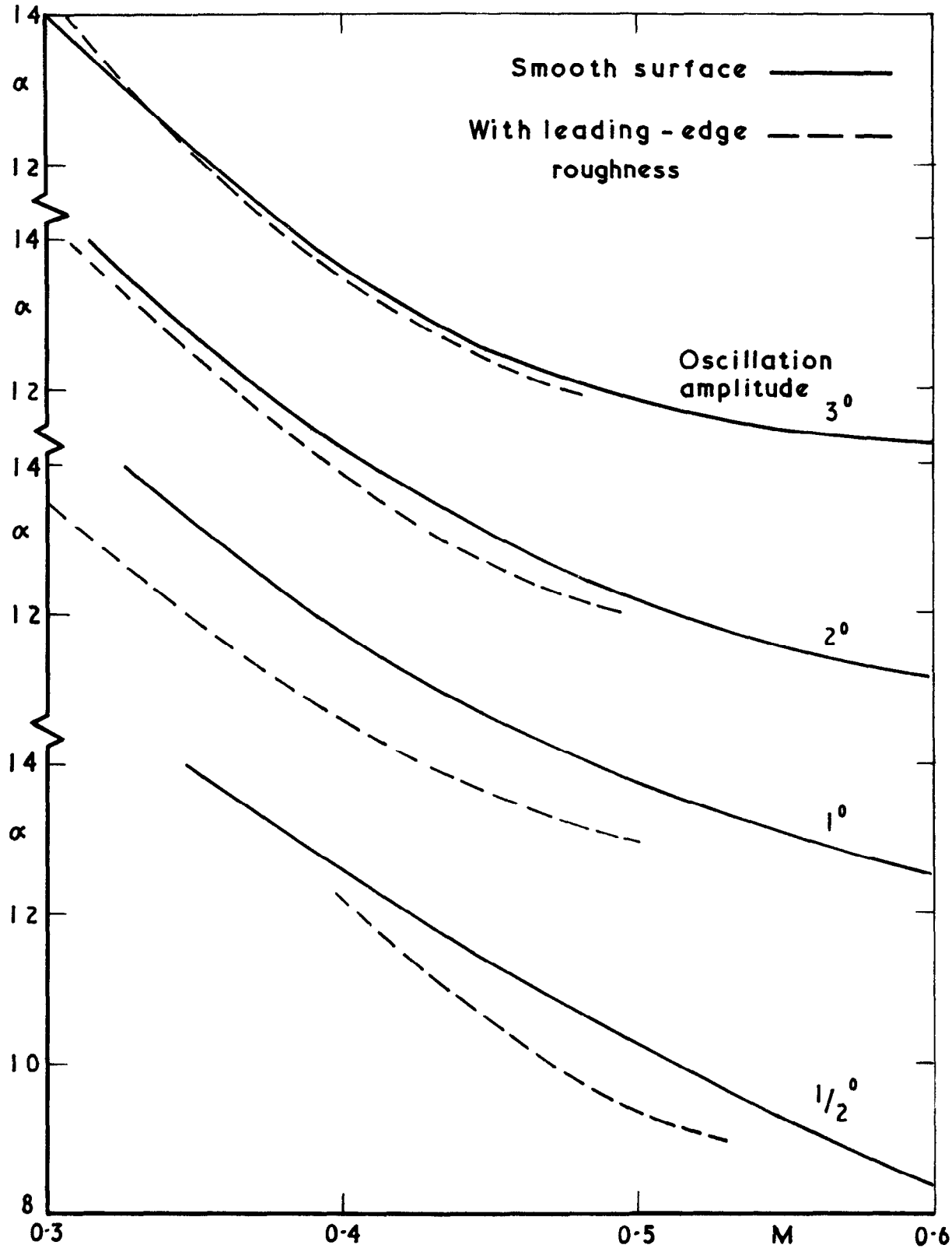

Fig. 16 Effect of leading-edge roughness on NACA 0012, 67 Hz

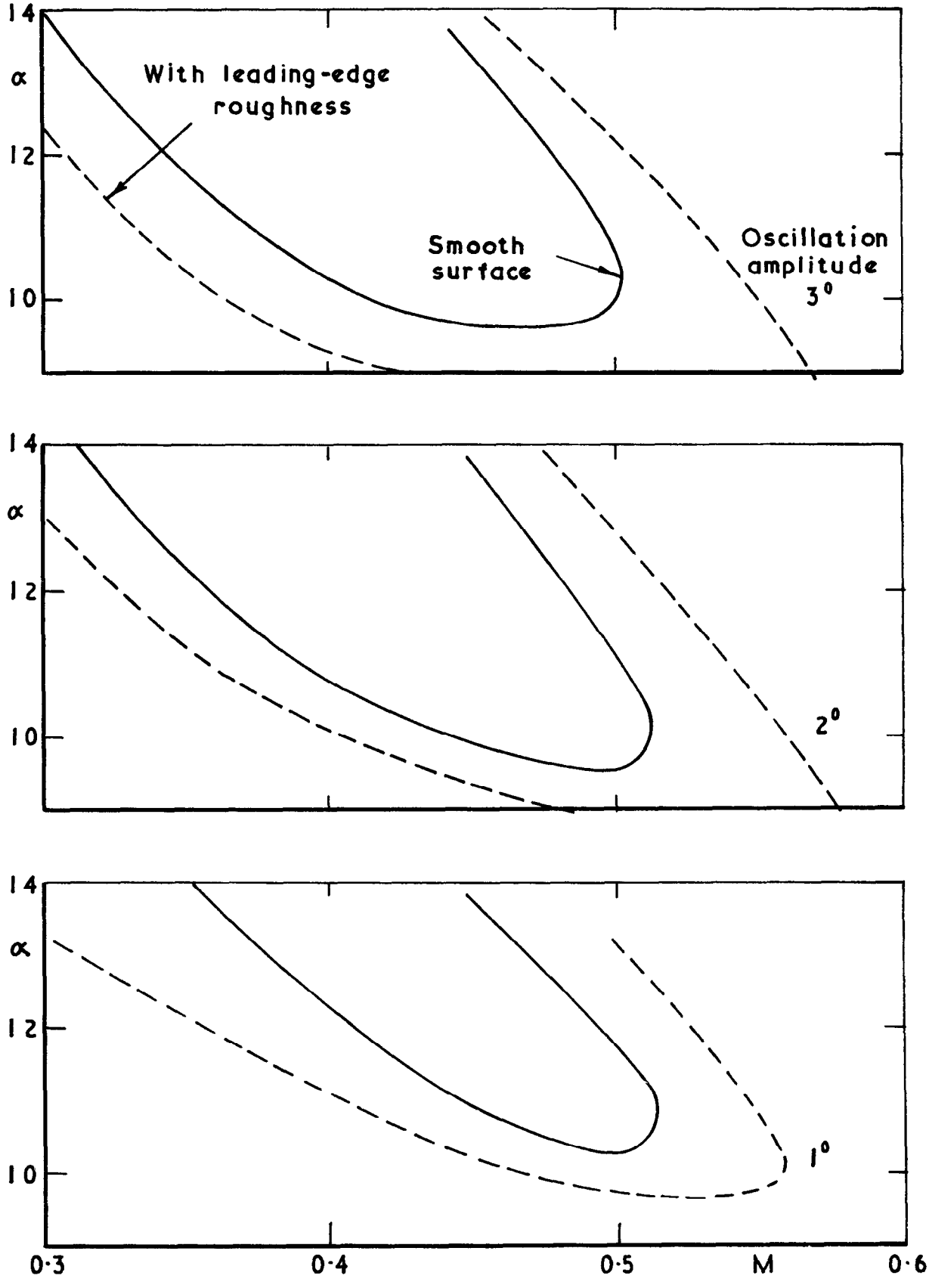

Fig.17 Effect of leading-edge roughness on NACA 0012; 43Hz

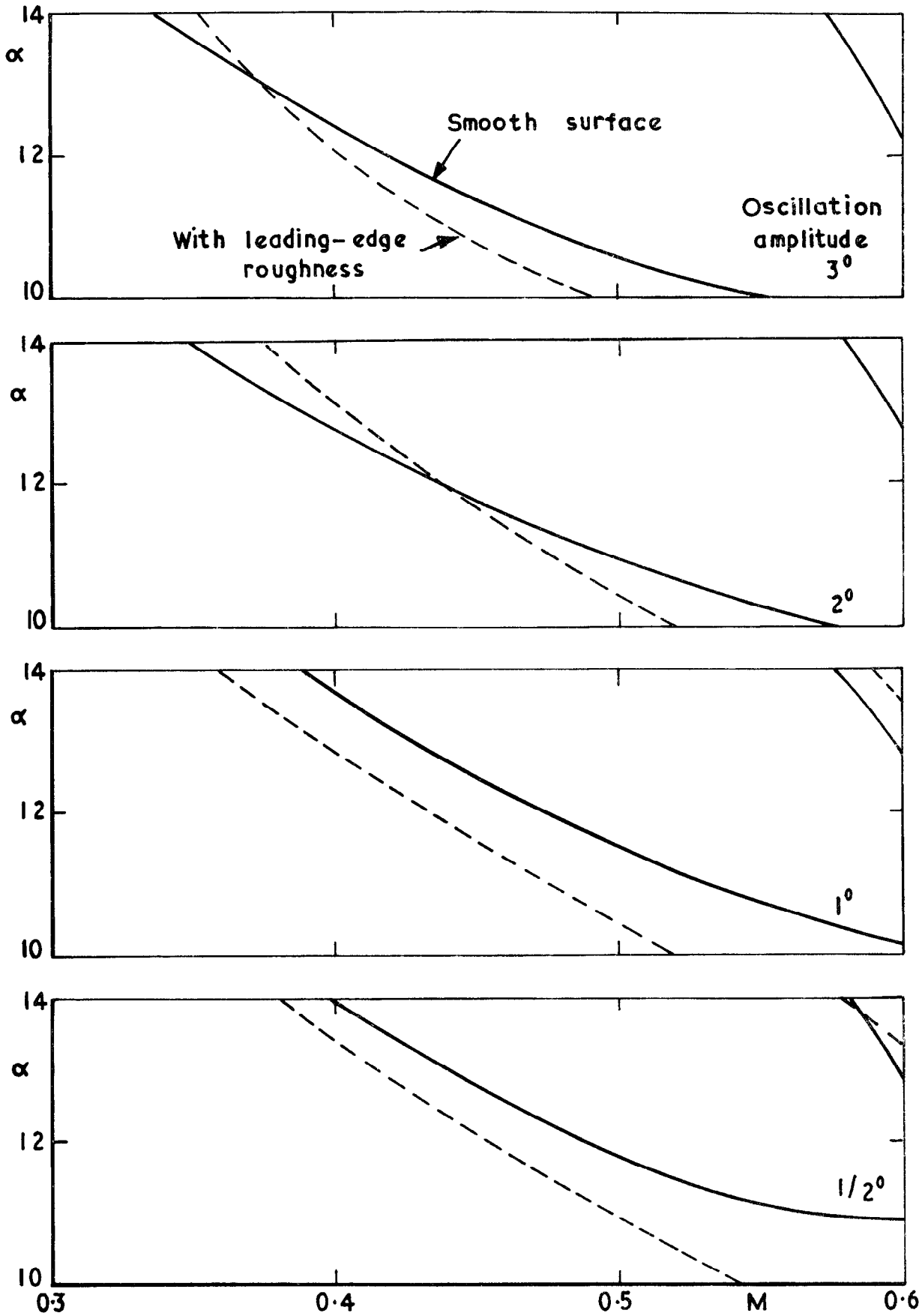

Fig.18 Effect of leading-edge roughness on NPL 9615; 67 Hz

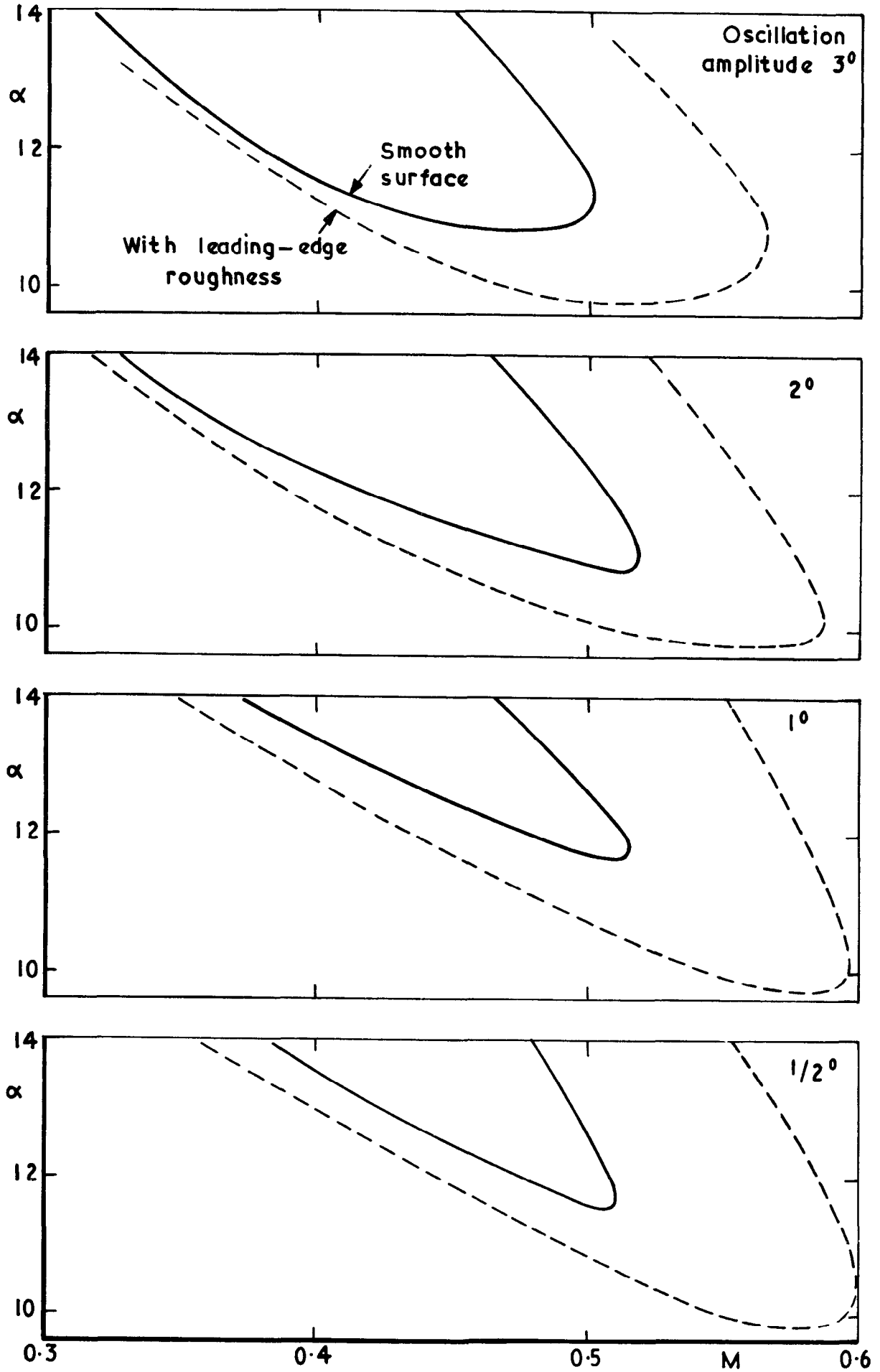

Fig.19 Effect of leading-edge roughness on NPL 9615; 43 Hz

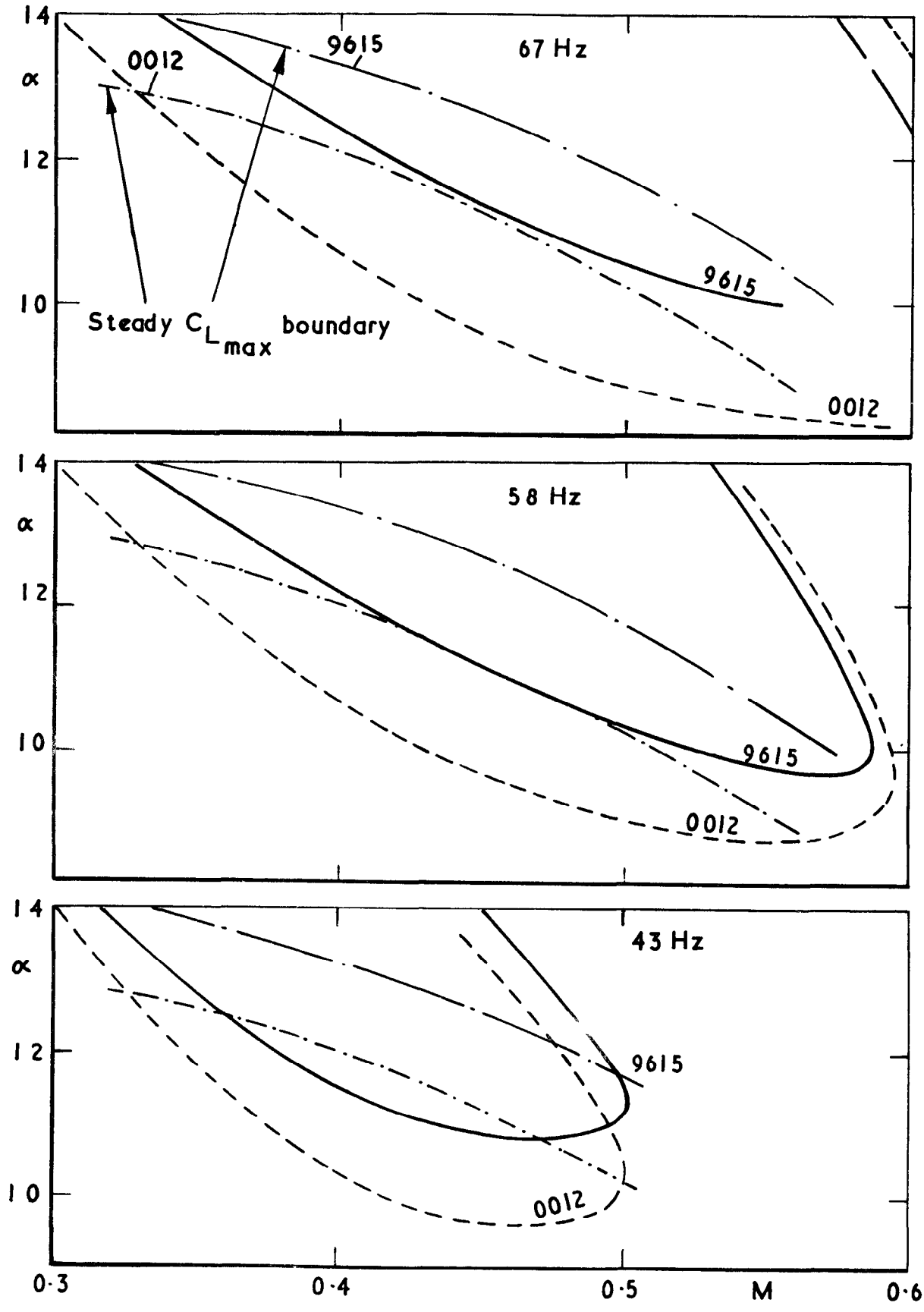

Fig·20 Comparison between stability boundaries for the two aerofoils with smooth surfaces; oscillation amplitude 3°

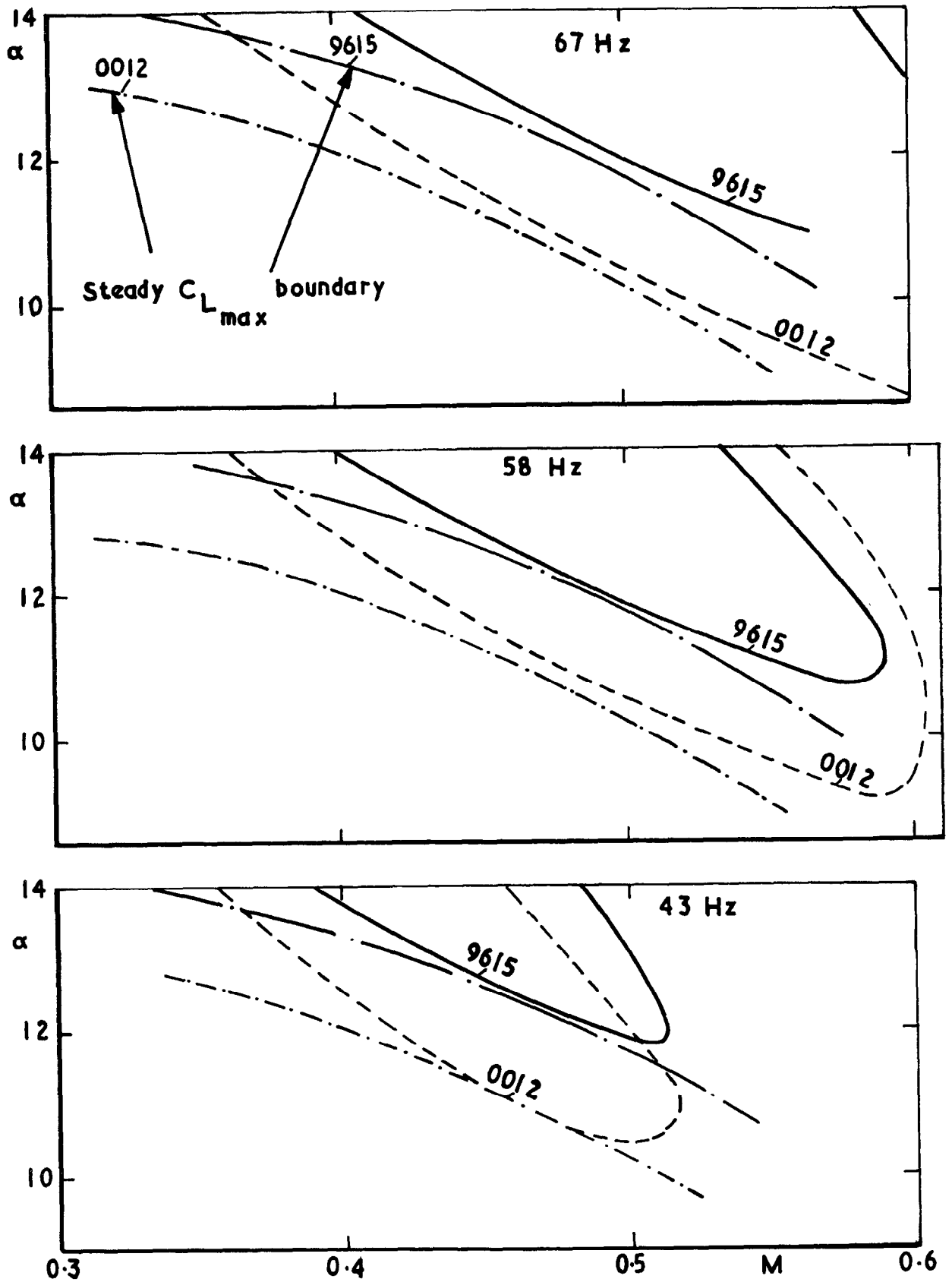

Fig. 21 Comparison between stability boundaries for the two aerofoils with smooth surfaces ; oscillation amplitude 0°

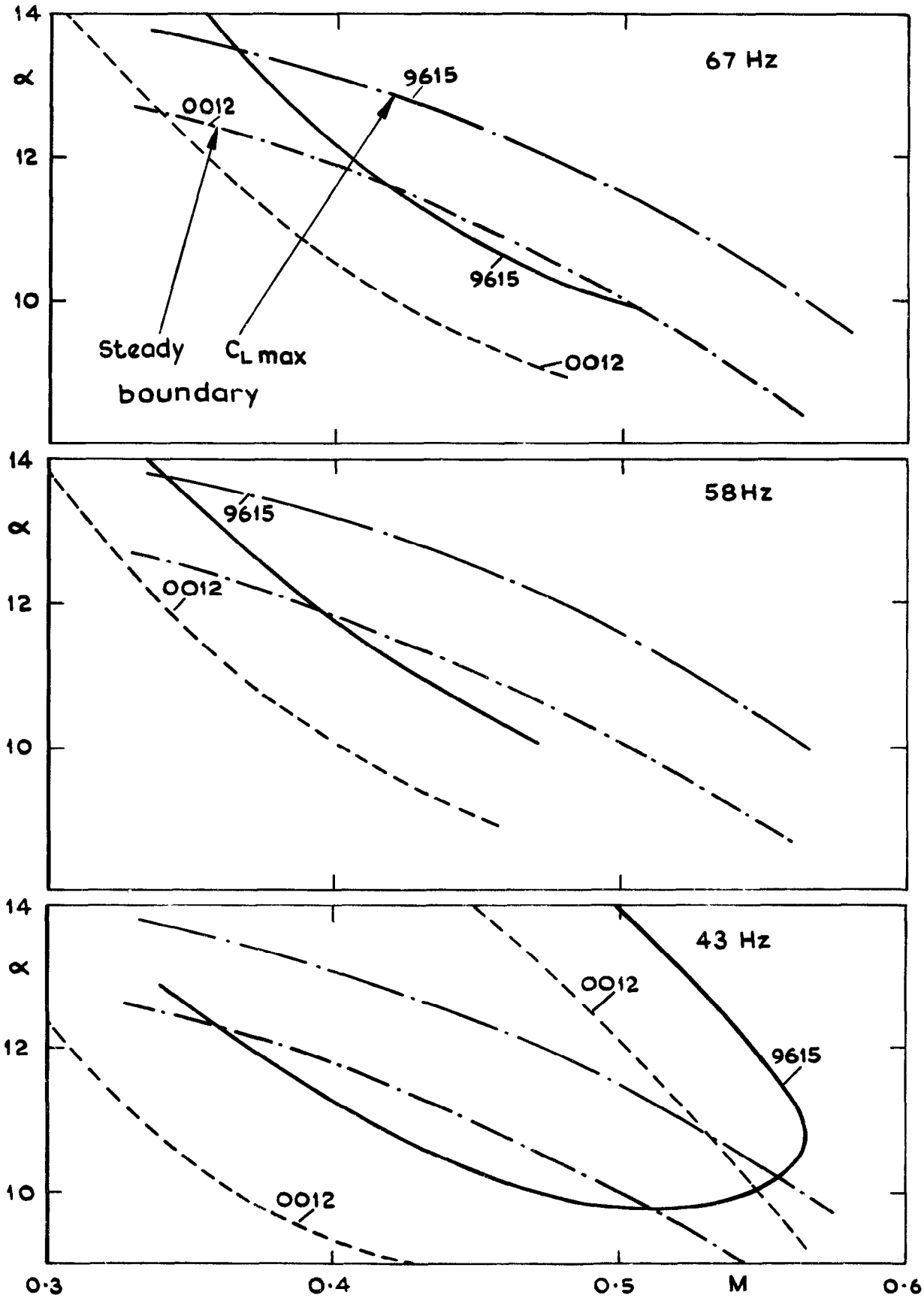

Fig.22 Comparison between stability boundaries for the two aerofoils with roughness added; oscillation amplitude 3°

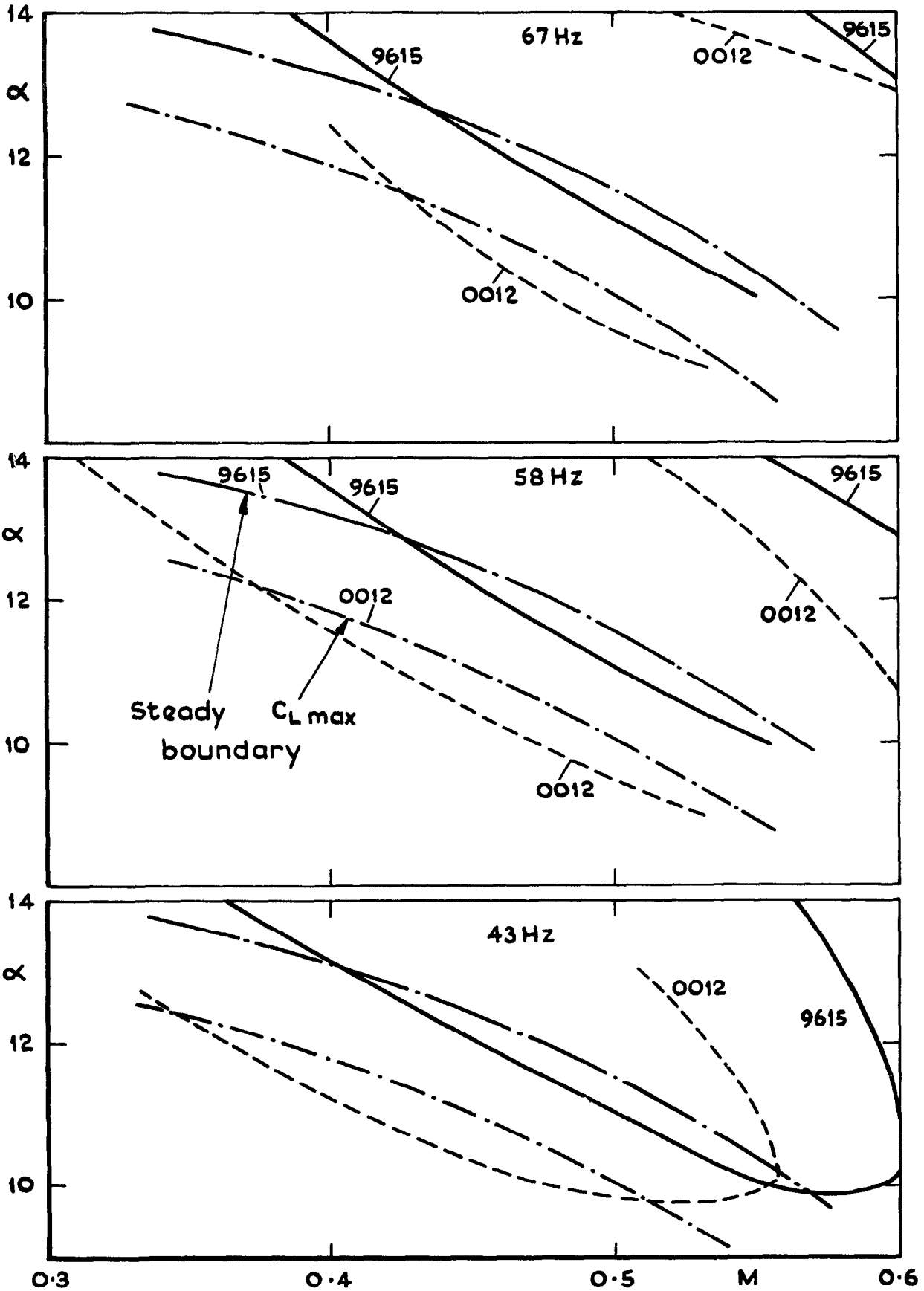

Note:- 0012 lower curve, 67 Hz, was estimated as extrapolation was not possible

Fig.23 Comparison between stability boundaries for the two aerofoils with roughness added; oscillation amplitude 0°

Printed in England for Her Majesty's Stationery Office by the Royal Aircraft Establishment, Farnborough. Dd. 505716 K4 12/73.

File

C.P. No. 1279

Published by
HER MAJESTY'S STATIONERY OFFICE

To be purchased from
49 High Holborn, London WC1V 6HB
13a Castle Street, Edinburgh EH2 3AR
41 The Hayes, Cardiff CF1 1JW
Brazennose Street, Manchester M60 8AS
Southey House, Wine Street, Bristol BS1 2BQ
258 Broad Street, Birmingham B1 2HE
80 Chichester Street, Belfast BT1 4JY
or through booksellers

C.P. No. 1279

ISBN 011 470863 0